Coordination Chemistry Reviews 253 (2009) 2835–2851

Contents lists available at ScienceDirect

Coordination Chemistry Reviews

journal homepage: www.elsevier.com/locate/ccr

Review

Polymer/clay and polymer/carbon nanotube hybrid organic–inorganic multilayered composites made by sequential layering of nanometer scale films

Paul Podsiadlo[a,1,2], Bong Sup Shim[a,1,3], Nicholas A. Kotov[a,b,c,*]

[a] Department of Chemical Engineering, University of Michigan, Ann Arbor, MI 48109, USA
[b] Department of Materials Science and Engineering, University of Michigan, Ann Arbor, MI 48109, USA
[c] Department of Biomedical Engineering, University of Michigan, Ann Arbor, MI 48109, USA

Contents

ARTICLE INFO

Article history:
Received 12 February 2009
Accepted 6 September 2009
Available online 12 September 2009

Keywords:
Layer-by-layer
Clay nanoparticles
Carbon nanotubes
Multilayered assemblies

ABSTRACT

This review article focuses on the preparation and applications of layer-by-layer (LBL) assembled organic/inorganic films. As model systems we use incorporation of two multi-functional nanomaterials in the LBL: the clay nanosheets and carbon nanotubes. All the aspects of the composite design starting with the structure of the individual nano-scale building blocks and their interactions with polymer matrix, orientation of the inorganic components in the multilayer, origin of record properties, and most likely applications of the resulting materials are given. Special attention is placed on the understanding of the control parameters for key functional properties such as mechanical strength/stiffness/toughness, electrical transport, transparency, and some properties relevant for biological applications.

1. Introduction

Nanotechnology has grown to be an area of research with tremendous scientific and economic potential. Just as the previous century has seen an explosion in the microprocessor and later biotechnology industries, this century is clearly becoming dominated by nanoscience. Nanomaterials can nowadays be synthesized with great control in respect to their composition, e.g. inorganic, organic, polymeric, biological, as well as structure and function.

* Corresponding author at: Department of Chemical Engineering, University of Michigan, 2300 Hayward St., Ann Arbor, MI 48109, USA. Tel.: +1 734 763 8768; fax: +1 734 764 7453.
E-mail address: kotov@umich.edu (N.A. Kotov).
[1] These authors contributed equally to this review.
[2] Current address: Argonne National Laboratory, Center for Nanoscale Materials, 9700 S. Cass Ave., Bldg. 440 A132C, Argonne, IL 60439, USA.
[3] Current address: Department of Materials Science and Engineering, University of Delaware, Newark, DE 19716, USA.

0010-8545/$ – see front matter © 2009 Published by Elsevier B.V.
doi:10.1016/j.ccr.2009.09.004

While there is still much work to be done in the basic synthesis and characterization of the building blocks, the next challenge of the field is transferring the nano-scale properties of these materials into macro-scale structures. Furthermore, multi-nano-component materials are now receiving growing attentions from diverse disciplines as noble complex materials systems equipped with, e.g. electro-opto-mechanical, chemo-electro-mechanical, and thermo-electrical properties [1].

Macro-scale assembly of the nanomaterials requires special techniques with molecular scale component manipulation, which is distinguished from conventional composite processing techniques like mix-and-molding and pre-preg layering. This nano-processing will intimately explore the chemical functionalities of the building blocks and enable nanometer-level control of organization in the superstructures. Among the different approaches being currently explored, the layer-by-layer (LBL) assembly technique stands out as one of the simplest and most versatile methods. In simplest of the cases, the technique is a method of alternating deposition of oppositely charged components from dilute solutions or dispersions on a suitable substrate. Since the first demonstration of LBL assembly for oppositely charged microparticles by Iler [2] and later by Decher et al. in the 1990s for oppositely charged polyelectrolytes [3,4], the LBL field has experienced rapid growth. The technique has quickly become one of the most popular and well-established methods for the preparation of multi-functional thin films not only thanks to its simplicity, but also robustness and versatility [5]. Introduction of hybrid organic/inorganic films has further enriched the functionality and applicability of LBL. Nearly any type of macromolecular species, including: inorganic molecular clusters [6], nanoparticles [7], nanotubes and nanowires [8,9], nanoplates [10], organic dyes [11], organic nanocrystals [12,13], dendrimers [14], porphyrin [15], polysaccharides [16,17], polypeptides [18], nucleic acids and DNA [19], proteins [20,21], and viruses [22] can be successfully used as assembly components [23]. Remarkable versatility has further led to a number of novel designs and applications, such as superhydrophobic surfaces [24,25], chemical sensors and semi-permeable membranes [23,26–28], drug and biomolecules delivery systems [23,29,30], memory devices [31], optically active and responsive films [13,32–34], cell and protein adhesion resistant coatings [23,35], fuel cells and photovoltaic materials [36], biomimetic and bio-responsive coatings [25,37], semiconductors [38,39], catalysts [40,41], and magnetic devices [42,43] and many more [5,23]. The technique has opened the door to an unlimited number of structural and functional combinations of colloids and macromolecules.

While the LBL field clearly covers a vast number of molecular species and architectures, in this review we concentrate on the state of the art in synthesis and properties of multilayer hybrid films based on two commercially available functional nanomaterials: the clay nanosheets and carbon nanotubes (CNTs). The two building blocks possess structural and physico/chemical properties unique to each, thus enabling preparation of variety of functional composites. Moreover, clay and carbon nanotubes are some of only few nanomaterials which allow evaluation of the efficiency of stress transfer in composites. This is because mechanical parameters of *individual* nanotubes and *individual* clay sheets are available. The review is accordingly divided into two sections covering the nanotubes and clays. Each section has subsections covering different research areas and applications of the resulting multilayers: (i) structure and properties of clays and CNTs; (ii) techniques for preparation of nanofilms; (iii) organization of the smectite particles in the nanofilms; (iv) organization of the adsorbed molecules; (v) functionalities of the films; (vi) other layered inorganic solids; and (vii) conclusions.

2. LBL assemblies of clays

2.1. Structure and properties of clay particles

The importance of utilization of clays in the LBL assemblies is threefold: (1) the natural abundance of this nanomaterial impart it with low cost; (2) the anisotropic, sheet-like structure is of great importance for control of transport properties through the films; and (3) like many other nanomaterials and given the single-crystalline, defect-free structure, the individual nanosheets possess exceptional mechanical properties, with in-plane modulus of elasticity (E) calculated on the order of ~270 GPa [44]. Before proceeding with actual overview of the clay multilayers, a few words need to be mentioned to the reader about the clays used in LBL assemblies.

The clays used in the LBL assembly are primarily layered silicates. The individual layer (nanosheet) is composed of a single layer of edge-shared octahedra of Al^{3+} or Mg^{2+}, sandwiched between two layers of corner-shared tetrahedra of Si^{4+} (Fig. 1). The thickness of individual sheet is ~0.96 nm and can be from tens to hundreds of nanometers in lateral dimensions. Substitutions in the tetrahedral and in the octahedral layers, i.e. partial replacement of Si^{4+} by Al^{3+} in the tetrahedral layers and of Al^{3+} by Mg^{2+} or Mg^{2+} by Li^{+} in the octahedral layers, create a negative lattice charge, which is compensated by exchangeable cations, e.g. Na^{+} or Ca^{2+}. The sheets are further organized face to face into aggregates. The exchangeable cations are localized in the interlamellar space between adjacent sheets of the aggregate.

In aqueous conditions, water molecules adsorb in the interlamellar space and disintegrate the stacks into individual sheets, which is called swelling or exfoliation. The extent of exfoliation depends on the size and charge of the cations. Extent of swelling is stronger for monovalent cations, such as Na^{+} or Li^{+}. For multivalent cations, e.g. Ca^{2+}, the attraction is stronger and exchange with water is more difficult and often incomplete.

2.2. Structural organization in clay multilayers

The first demonstration of LBL assembly of clay nanosheets with polyelectrolytes (PEs) was given by Kleinfeld and Ferguson in 1994 [46,47]. The authors used a strongly charged PE which is common nowadays in the LBL field, the poly(diallyldimethylammonium chloride) (PDDA, Fig. 2A) and a synthetic clay, hectorite (Laponite RD) to grow few-hundred-nanometers-thick films. In the course of study the authors used optical ellipsometry to follow growth of the multilayer deposited on a Si substrate (Fig. 2). They observed linear increase in thickness with an average increment per bilayer of ~3.6 nm. Additionally, they also observed highly uniform surface coverage of the substrate with visible Bragg diffraction colors, which were further indications of uniformity of the structure. X-ray diffraction (XRD) spectra demonstrated structural ordering in the multilayer, with clay sheets being adsorbed in a periodic multilayer with parallel orientation of the sheets with respect to the substrate. The clay nanosheets adsorbed as single lamella and there were no 3D aggregates in the structure. This first demonstration opened the road to the subsequent studies on clay multilayers.

Several research groups have subsequently aimed at more detailed characterization of the adsorption kinetics, organization, and control of the internal structure of the clay/PEs films. The structure and surface roughness of LBL assembled films was depended on several parameters including adsorption time, concentration of cationic polymer, amount of clay in the dispersion and pH. As an example, Lvov et al. extended the preparation of clay multilayers to PDDA/montmorillonite clay (MTM) and poly(ethyleneimine) (PEI)/MTM systems [48,49]. They also studied adsorption kinetics by quartz crystal microbalance (QCM). The adsorption of MTM

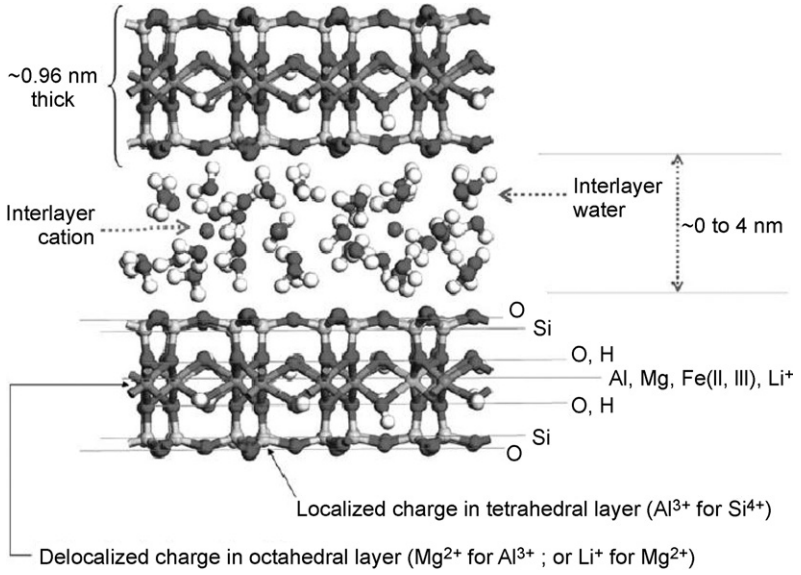

Fig. 1. Structure of layered silicates (figure was reproduced from Ref. [45], with permission of the copyright holders).

clay was saturated in 5–6 min with formation of a monolayer of platelets, with shorter times leading to incomplete surface coverage and longer times resulting in physisorption of extra platelets. Kotov et al. performed further detailed studies on interaction of MTM with PDDA and the self-assembly process by surface plasmon spectroscopy, XRD, and X-ray reflectivity (XRR), and atomic force microscopy (AFM) [50]. They gave insightful details into the self-assembly process and defect formation in the films. They also showed that surface roughness of the films was independent of the underlying substrate and that the roughness could be controlled to some extent with an application of external voltage during adsorption of the PE. Negative bias produced more regular and uniform self-assembled films.

Another parameter controlling the morphology of the films is the concentration of PE. van Duffel et al. observed that the surface roughness of clay-polymer LBL multilayers increases with cationic polymer concentration in solution [51]. As an explanation, they suggested that at low polymer concentration the polymer chains can bind strongly clay platelets, resulting in stretched chains and a small number of unbound polymer units. This film has a low surface

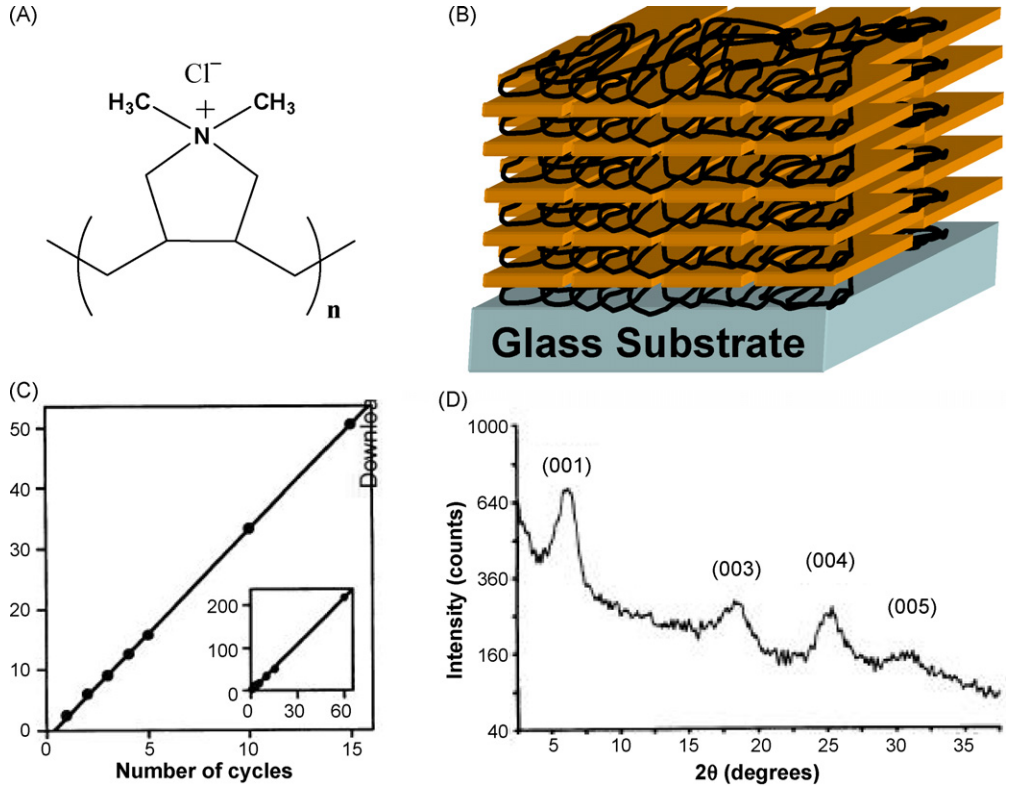

Fig. 2. (A) Chemical structure of PDDA. (B) Idealized view of internal architecture in polymer/clay multilayer composed of 5.5 bilayers. (C) Ellipsometric films thickness (nm) as a function *f* number of deposited layers. Inset shows linearity of growth up to 60 bilayes. (D) X-ray diffraction spectrum of a 60-bilayer sample of PDDA/Hectorite indicating periodic internal organization (figure was reproduced from Ref. [46], with permission of the copyright holders).

roughness. For high PE concentrations, multiple polymer chains are only partially bonded to the substrate and are sticking out of the surface. Bundles of clay platelets can adsorb under these conditions, being more or less stacked on top of each other. This results in a rough film surface.

Laschewsky's group studied the influence of PE charge density on the multilayer growth [52]. They showed that multilayers composed of a strong polyanion, namely poly(styrenesulfonate) (PSS) and cationic copolymers of PDDA with *N*-methyl-*N*-vinylformamide (NMVF), with varied charge density, had a critical linear charge density λ_c of 0.036 elementary charge/Å of contour length in order to obtain stable multilayer growth in pure water. Above λ_c, the increment of thickness/deposition cycle varied with the linear charge density of the cationic copolymers. As linear charge density increased, the system passed successively through a charge-dependent "Debye-Hückel" regime and then through a charge-independent "strong-screening" regime where counterion condensation dominated the behavior. Analogous results were obtained by the authors for the variation of the basal spacing of internally structured hybrid multilayers (cationic copolymer/hectorite). However, by contrast with the PEs system, no critical linear charge density was observed in the hybrid system. This was explained by additional, nonelectrostatic interactions between the clay platelets and the formamide fragment.

The same group further explored the potential for forming PE/clay multilayers incorporating copolymers to produce films from UV cross-linkable PEs [53]. They found that the photoreaction reduced the films' roughness and promoted more regular growth. From a practical point of view, they suggested that this approach could offer additional benefits for the clay multilayers, such as improving the barrier functionality of the inorganic layers as well as the control of the permeability between pure organic sublayers. Furthermore they studied preparation of multilayers from derivatives of PDDA [54]. They synthesized a series of PDDA polymers with varying hydrophilic/hydrophobic balance and bulkiness of the cationic group, to investigate impact of the parameters on the formation of LBL assemblies with Laponite (Fig. 3). They found that bulky and hydrophobic, as well as amphiphilic, polycations could be accommodated between the rigid exfoliated aluminosilicate platelets without disturbing the lamellar-like structure. Ellipsometry and XRR showed that hydrophobic and bulky substitution favored formation of thicker films, due to more coiled conformation of the PEs. Films showed partial organization and coherence lengths along the normal of the plane, in the range of 2.7–7.5 nm. The values depended sensitively on the detailed chemical structure of the PE employed.

Since the clay multilayers are prepared in aqueous conditions, an important parameter of interest for applications of the resulting structures is their stability in the aqueous environment. Rouse and Ferguson recently used XRD to study water sorption in PDDA/Laponite multilayers [55]. Interestingly, they found that swelling occurred exclusively in X-ray amorphous regions within the film, and that the ordered PDDA/clay domains themselves were not affected by water. Clearly, one can imagine that the swelling characteristics will be dependent on the chemical structure of the PEs, the nature of interactions at the organic/inorganic interface, as well as post-assembly treatments, e.g. covalent cross-linking of the multilayer.

So far we have discussed preparation of the multilayers from negatively charged clays. Recently, several groups have also investigated LBL assembly from positively charged, synthetic clays called "layered double hydroxides" (LDH). The synthetic clays offer new opportunities for functional assemblies, e.g. optical, magnetic, or catalytic, since different combinations of ions can be artificially introduced into the nanosheet gallery. Li et al. for the first time showed LBL assembly of Magnesium–Aluminum LDH nanosheets with anionic polymer PSS [56]. They studied assembly with UV–vis and XRD techniques. The same group has further synthesized Cobalt–Aluminum LDH in the form of hexagonal platelets and used them for LBL assembly with PSS [57]. The new type of LDH showed significant magneto-optical response in the UV–vis regime. Szekeres et al. have also demonstrated successful assembly of Magnesium–Aluminum LDH with PAA and PSS [58]. The authors studied LBL assembly with surface plasmon resonance. Preparation of multi-LDH, transparent LBL multilayers containing stratas of Magnesium–Aluminum and Cobalt–Aluminum LDH's, as well as a new Nickel–Aluminum derivative was also recently demonstrated [59]. The incorporation of transition metals into the LDH nanosheets offers new opportunities for preparation of novel catalytic membranes. In a most recent study, Altuntasoglu et al. showed preparation of an even more exotic LDH, the Nickel–Gallium [60]. LBL multilayers of the Nickel–Gallium LDH exchanged with ferricyanide with PAA showed typical response of metal hexacyanoferrate, which was believed to be formed in the interlayer.

Finally, in respect to the internal organization of the films, we should mention two most recent cases of PE/clay preparation which deviate from traditional dipping and/or monolayer deposition and have important implications for structural organization of the clay and PE layers. The first case is related to the preparation of the multilayer using spin-assisted self-assembly. In this process, instead of dipping of the substrate into the solutions of constituents, the solutions are alternately spin-coated onto the substrate with intermediate rinsing steps with pure water. The consequences of large centrifugal forces, short contact times, and rapid solvent evaporation are not clear in respect to multilayer formation. Recently, Lee et al. showed the first successful preparation of clay multilayers by spin-assisted self-assembly [61]. The authors used poly(*p*-phenylene vinylene) (PPV) and Laponite clay and characterized the resulting structure by contact angle measurement, surface dying technique, UV–vis spectroscopy, photoluminescent (PL) spectroscopy, XRR, and model-fitting. The continuous increase of UV–vis absorbance and PL intensity of the films with each bilayer demonstrated the regular and reproducible deposition of this system, and the Kiessig fringes and Bragg peaks in XRR spectra indicated the well-ordered internal structure. Subsequently, Vertlib et al. also showed robust and fast preparation of Laponite/PDDA LBL films by spin-assisted self-assembly with high mechanical properties.

In the second case, we recently showed that MTM nanosheets can be successfully incorporated into so called "exponential" LBL assembly (e-LBL) of PEI and poly(acrylic acid) (PAA) which leads to novel architectures [62]. The e-LBL mode was first characterized by Picart et al. and it is has been associated with "in-and-out" diffusion of PEs through a swollen multilayer structure [63]. Incorporation of MTM sheets was believed to hinder the diffusion process and thus prevent the e-LBL growth. In spite of this expectation, we showed that MTM nanosheets could be successfully incorporated and that the diffusing PEs can potentially help exfoliate the short stacks of MTM into single lamella. The internal ordering of the film was substantially decreased as revealed by small-angle x-ray scattering (SAXS) and scanning electron microscopy (SEM) (Fig. 4), however the e-LBL mode offers new opportunities for preparation of multilayers with unique internal organization.

2.3. Clay multilayers as high-performance nanocomposites

One of the unique perspectives for clay multilayers is their potential as high-performance nanocomposites. As we mentioned in the beginning of this section, clay nanosheets possess exceptional mechanical properties. MTM nanosheets, for example, have in-plane modulus of elasticity on the order of ~270 GPa [44] if

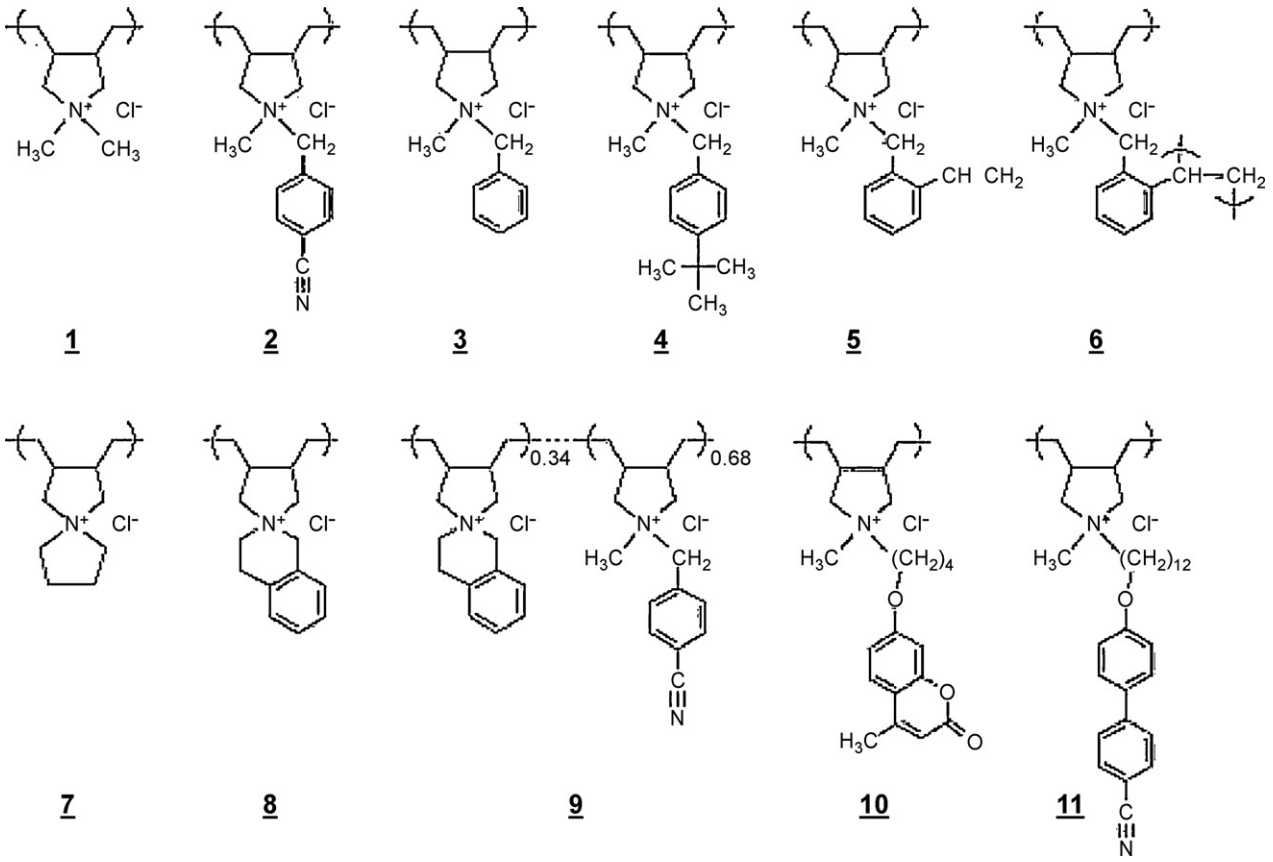

Fig. 3. Poly(diallylammonium) salts used as organic counter-polycations of negatively charged Laponite platelets for the preparation of hybrid multilayers (figure was reproduced from Ref. [54], with permission of the copyright holders).

we consider the gallery of ions, which is comparable to steel and its alloys (E = 210 GPa), yet at much lower density. Given the high mechanical properties, low cost, and large surface areas, clays have been extensively investigated as reinforcing fillers for enhancing mechanical properties of commercial plastics [64]. Significant enhancements of strength, Young's modulus (E), and toughness have been observed upon addition of just a few volume percentages of the inorganic filler. However, above the few percentiles (usually more than 10 vol.%), the mechanical properties begin to deteriorate due to strong tendency of clay particles to phase segregate and aggregate, thus creating fatal defects. The clay multilayers show an interesting promise for overcoming these problems thanks to a number of advantages: (1) the nanocomposites are constructed by alternately depositing nanometer-thick layers of polymer and clay, thus allowing for nanometer-level control of preparation; (2) alternating the layers of clay nanosheets with few-nanometer-thick layers of polymers translates into volume fractions upwards of 50 vol.%; (3) the colloidal self-assembly process restricts adsorption of clay to well-exfoliated sheets; and (4) sandwiching of the nanosheets between polymer layers and strong interfacial bonding prevent phase segregation of the nanofiller.

Kotov et al. have realized for the first time that PDDA/MTM multilayers had unusually high strength, flexibility, and resistance to crack propagation [65]. The authors observed that individual nanosheets possessed high flexibility to bending which further translated into flexibility of the film itself. This was an interesting development, especially given the enormous tangent stiffness of individual platelet (~270 GPa). The authors realized that individual nanosheets behave more like pieces of a flexible fabric. High mechanical properties were of paramount importance for utilization of these films as ultrathin separation membranes. The flexibility and high strength of the PDDA/MTM multilayers was further utilized by Mamedov et al. for preparation of multi-functional free-standing membranes [43]. In this work, the authors incorpo-

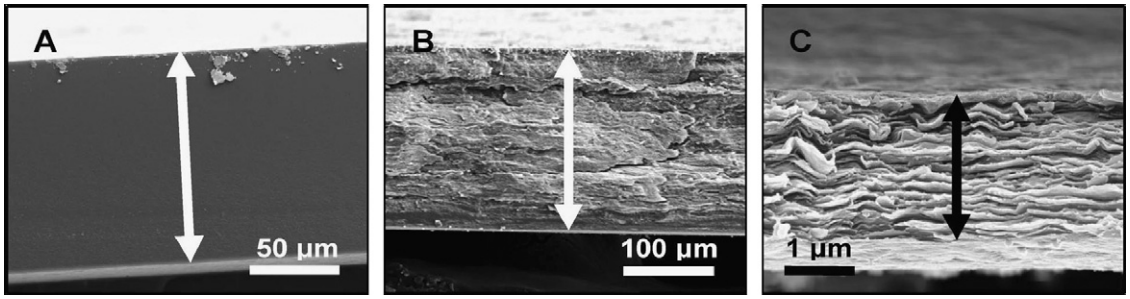

Fig. 4. SEM images of cross-sections for free-standing films of (A) $(PEI/PAA)_{200}$, (B) $(PEI/PAA/PEI/MTM)_{100}$, and (C) $(PEI/MTM)_{100}$. Arrows indicate span of the cross-section (figure was reproduced from Ref. [62], with permission of the copyright holders).

rated the MTM sheets into a LBL assembly of PDDA and magnetite nanoparticles. The clay layers were introduced by replacing every second layer of magnetite with MTM. The clay nanosheets imparted substantial improvement of strength over the films without MTM. Using a similar concept, Hua et al., have recently developed ultrathin cantilevers for sensing applications [66]. The cantilevers were composed from six alternating monolayers of MTM, PDDA, and magnetite nanoparticles and they were 170-nm thick.

The two singular observations led our and other groups to further investigate the mechanical properties of PDDA/MTM composite films. Advincula's group for example, investigated mechanical properties of the films with nanoindentation [67]. The hardness (H) and modulus of the films was $H = 0.46$ GPa and $E = 9.5$ GPa, respectively. The thin film's modulus was correlated to its ordering and anisotropic structure. Both hardness and modulus of this composite film were higher than those of several other types of polymer thin films. Furthermore, Tang et al. prepared a series of free-standing films with 50, 100, and 200 bilayers and tested mechanical properties of the films with standard stretching techniques [68]. He found the ultimate strength (σ_{UTS}) and modulus, $\sigma_{UTS} = 100 \pm 10$ MPa and $E = 11 \pm 2$ GPa. The material was stronger and stiffer than some of the strongest commercial plastics and the enhancement of strength and stiffness over the base PDDA polymer was nearly 10× and 50×, respectively. Additionally, under low strain rates (slow stretching) the films exhibited a toughening behavior, evidenced by unusually high strain (ε) values of, $\varepsilon \sim 10\%$. Analysis of the differential of the stress–strain curve revealed a "saw-tooth" pattern, which was an evidence of breaking and reforming of ionic bonds between PDDA and MTM surface (Fig. 5). Similar behavior was observed in one of the toughest natural composites called "nacre". Having analogous architecture, strength (σ_{UTS} of nacre is ~110 MPa), and deformation mechanics, the composite was dubbed "nanostructured artificial nacre".

The realization of exceptional potential of the PE/MTM composites prompted us to further investigate mechanical properties of this new class of composites. In an attempt at developing even stronger materials based on this architecture and to better understand the nano-scale and molecular mechanics of the composites, we have explored different compositions of the films and hypotheses. The well-ordered multilayer structure served as a model system for investigating nano-scale mechanics in polymer/clay composites.

In the first attempt, we replaced PDDA with a biopolymer with nearly and order of magnitude greater strength and stiffness, the Chitosan (Fig. 6) [69]. Contrary to our expectations and in spite of uniform architecture, the composite showed lower σ_{UTS} and E when compared to PDDA/MTM. Detailed investigation of the system led us to a conclusion that molecular rigidity of Chitosan's chains prevented formation of well-interlocked structure, and thus decreased interfacial interactions with MTM. With this result in mind, we have further investigated improvement of interfacial interactions by replacing PDDA with a flexible poly(ethylene glycol) (PEG) star polymer containing L-3,4-dihydroxyphenylalanine (DOPA) adhesive groups found in mussels [70,71]. This was the first exemplary structure where concepts found in two different natural materials were combined to produce a superior composite. An important development in this structure was utilization of a hardening mechanism found in mussels, i.e. cross-linking of DOPA molecules to each other with Fe^{3+} ions. The cross-linking has led to substantial improvement of mechanical properties, with σ_{UTS} increasing to ~200 MPa.

Following the discovery of enhancement of the mechanical properties upon post-assembly cross-linking, we turned our attention to another polymer, poly(vinyl alcohol) (PVA). PVA has a simple chemical structure with repeating hydroxyl groups attached to every other carbon atom in the polymer's backbone (Fig. 6). Important feature of the hydroxyl groups is that they can be easily cross-linked covalently and ionically. The PVA chains are also uncharged; hence a question arose as to the feasibility of LBL assembly with MTM. Surprisingly, the assembly was robust and the resulting free-standing films showed record-high mechanical properties for clay nanocomposites, especially after covalent cross-linking with glutaraldehyde (GA). They also had nearly 90% optical transparency [72]. The resulting tensile strength was, $\sigma_{UTS} = 400 \pm 40$ MPa and stiffness of $E = 106 \pm 11$ GPa. Detailed spectroscopic investigation revealed that PVA groups were epitaxially binding to the surface of clay sheets and GA cross-linking was also covalently binding MTM sheets with polymer, thus enhancing the transfer of mechanical properties. Furthermore, the covalent cross-linking rendered the composite water-inert. Similarly with ionic cross-linking, we found that Al^{3+} and Cu^{2+} gave substantial enhancements of mechanical properties, with σ_{UTS} reaching as high as 320 MPa and E of nearly 60 GPa [73].

These results showed tremendous promise of LBL technique for preparation of high-strength clay nanocomposites. However, slow deposition speeds are currently limiting these materials to applications in coatings and thin membranes. Our group is currently investigating preparation of laminated composites from the ultrastrong sheets, but two most recent developments, which we have discussed in the previous section, are already carrying a promise for accelerating the preparation of composites. In the first, the e-LBL assembly, we found from nanoindentation that the films had high hardness and stiffness, even though the content of MTM sheets was dramatically lower when compared to linear LBL [62]. The modulus and hardness were on the order of, $E = 16$ GPa and $H = 0.88$ GPa, and they were more than 50% greater than those reported by

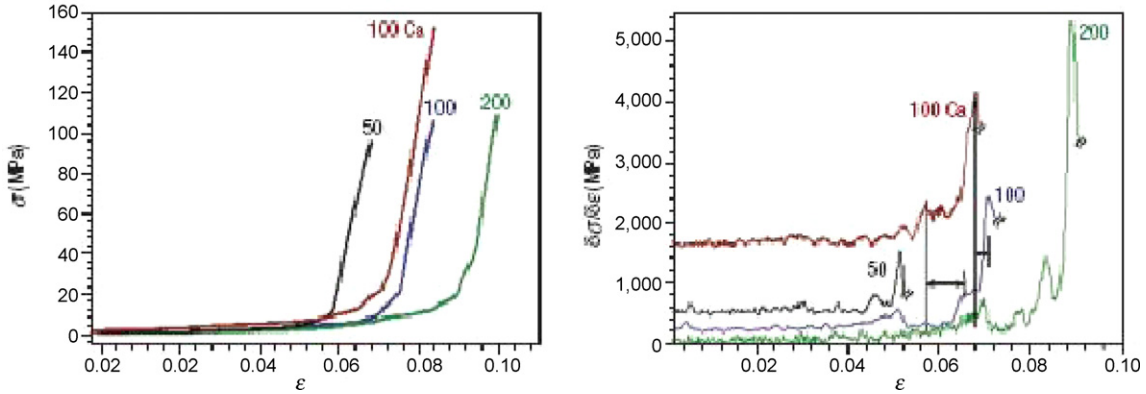

Fig. 5. Tensile behavior of PDDA/MTM free-standing films (left) and corresponding derivatives of the stress–strain curves (right) (figure was reproduced from Ref. [68] with permission of the copyright holder).

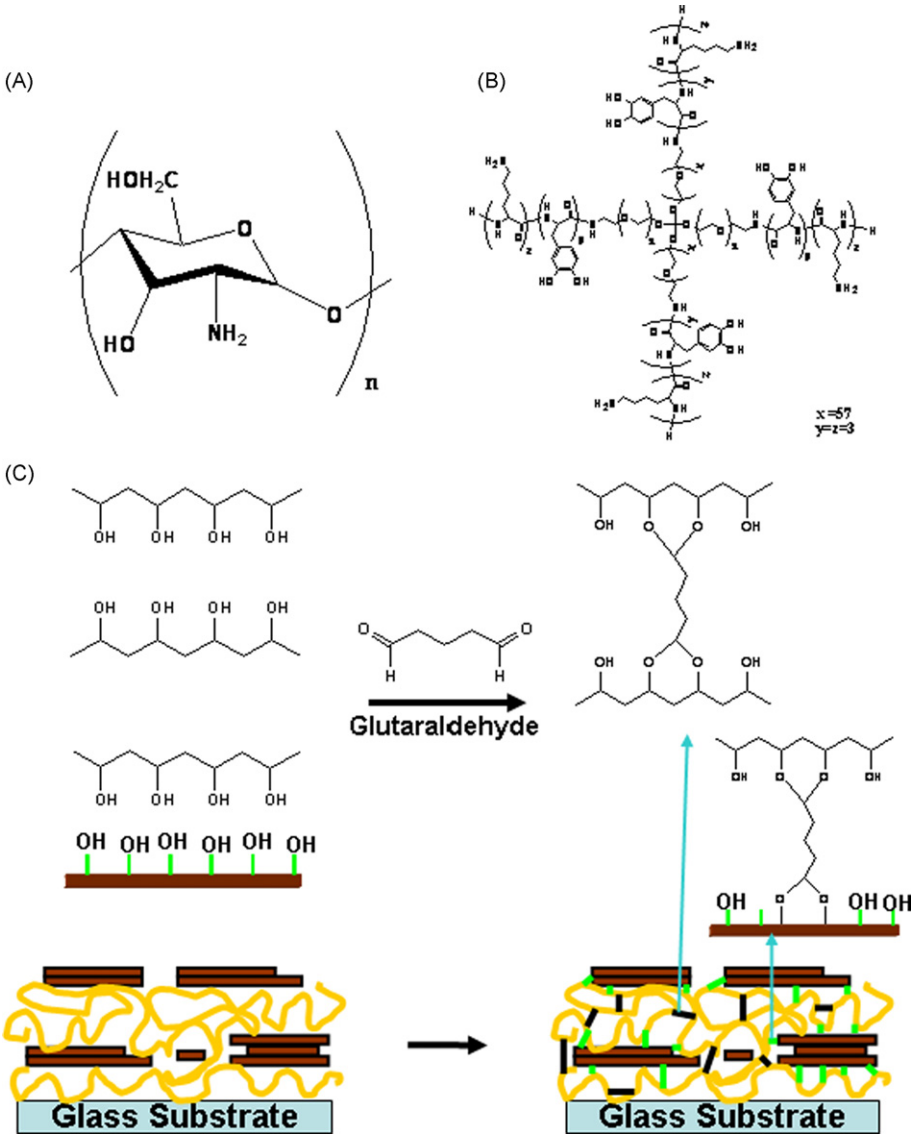

Fig. 6. (A) Chemical structure of Chitosan. (B) Chemical structure of PEG containing DOPA molecules (figure was reproduced from Ref. [71] with permission of the copyright holder). (C) Chemical structure of poly(vinyl alcohol) and basis of chemical cross-linking with MTM sheets (figure was reproduced from Ref. [72] with permission of the copyright holder).

Advincula for PDDA/MTM. The film growth was nearly 100× faster when compared to linear LBL. In the second case, spin-assisted LBL was recently used by Vertlib et al. for accelerating assembly of PDDA/Laponite composites [74]. The authors found that the mechanical properties of the resulting films were approaching those obtained from dip-coating LBL, with $H \approx 0.44$ GPa and $E \approx 8$ GPa, yet with 10× faster deposition speed.

2.4. Applications of clay multilayers in biotechnology

The mechanical properties of clays have great importance for variety of applications. The natural origins and bio-inert composition impart them with additional advantages for biomedical constructs. The first application of the clay multilayers for this purpose was demonstrated by Lvov et al. [48,75,76]. The authors demonstrated the first preparation of multilayer films containing more than one protein species in combination with positively charged PEI or with negatively charged PSS, as well as MTM. The proteins used were water-soluble cytochrome *c*, myoglobin (Mb), lysozyme (Lys), histone f3, hemoglobin (Hb), glucoamylase, and glucose oxidase (GOD). They have monitored the assembly by QCM and UV-vis spectroscopy. Importantly, a multilayer consisting of alternating MTM, PEI, and GOD layers was also assembled (Fig. 7A). This biomolecular architecture opened a way to construct artificially orchestrated protein systems that could carry out complex enzymatic reactions.

Soon after, Zhou et al. prepared stable LBL films from Bentonite clay and Hb on various solid substrates by alternate adsorption of negatively charged clay platelets from their aqueous dispersions and positively charged Hb from pH 4.5 buffers [77]. They used cyclic voltammetry (CV), QCM, and UV–vis spectroscopy to monitor film growth. CV of $(clay/Hb)_n$ films on pyrolytic graphite electrodes showed a pair of well-defined, nearly reversible peaks at about −0.27 V vs. saturated calomel electrode (−0.02 V vs. normal hydrogen electrode) at pH = 5.5, characteristic of the $HbFe^{III}/Fe^{II}$ redox couples (Fig. 7B). Although the amount of Hb adsorbed in each bilayer was essentially the same, the fraction of electroactive Hb decreased with the number of clay/Hb bilayers (n). Electroactivity of Hb extended to six clay/Hb bilayers (Fig. 7C). The Soret absorption band of Hb in $(clay/Hb)_6$ films showed that Hb retained its secondary structure similar to its native state in the medium pH range. A Bragg peak in XRD for $(clay/Hb)_{20}$ films suggested a

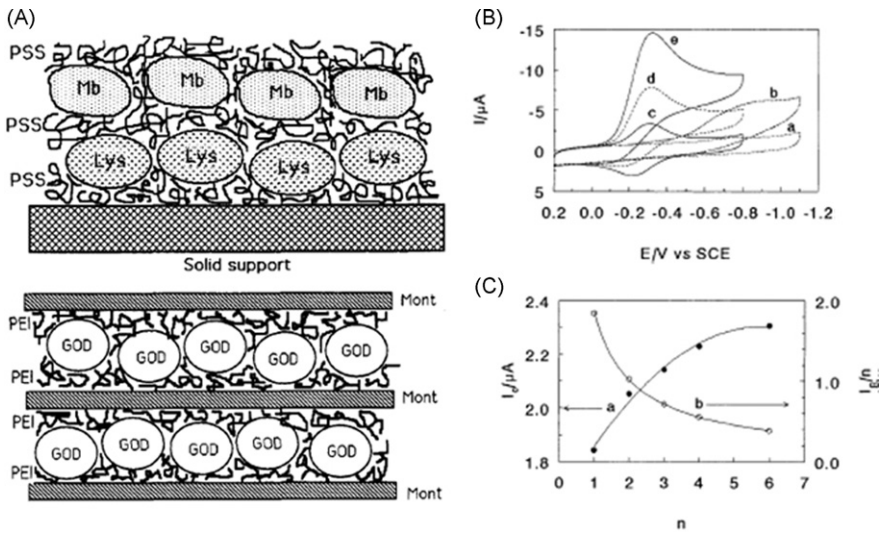

Fig. 7. (A) Schematic simplified illustrations of protein films: (top) Mb/PSS/Lys/PSS multilayer and (bottom) GOD/PEI/MTM/PEI multilayer (figure was reproduced from Ref. [75], with permission of the copyright holder). (B) Cyclic voltammograms at 0.2 V s^{-1} in 9 mL of pH 5.5 buffer solutions for (a) clay monolayers with no oxygen present, (b) clay monolayers after 30 mL of air was injected in a sealed cell, (c) $(clay/Hb)_6$ films with no oxygen present, (d) $(clay/Hb)_6$ films after 30 mL of air was injected, and (e) $(clay/Hb)_6$ films after 60 mL of air was injected (figure was reproduced from Ref. [77], with permission of the copyright holder). (C) Influence of number of bilayers (n) on (a) catalytic peak current (I_c) and (b) average catalytic peak current per bilayer (I_c/n) for $\{clay/Hb\}_6$ films; 10 mM TCA in pH 3.0 buffers, scan rate of 0.08 V s^{-1}.

partly ordered, layered structure of the films, but without full Hb intercalation. $(Clay/Hb)_6$ film electrodes were further successfully used to catalyze the electrochemical reduction of trichloroacetic acid, oxygen, and hydrogen peroxide. In further studies Li and Hu have also reported direct electrochemistry of heme proteins in LBL assemblies with MTM [78] and Lojou with Bianco [79] reported LBL assemblies of MTM and bacterial cytochromes for bioelectrocatalytic devices.

Besides the electrocatalytic activity, clay multilayers have also been used as interfaces/substrates for cell culture. Recently we showed that a combination of PDDA, MTM, and starch stabilized, negatively charged Ag nanoparticles, allows for preparation of a strong, nacre-like composite LBL coating with good biocompatibility and antibacterial activity simultaneously [80]. Strong electrostatic interactions imparted good stability to the coating under aqueous conditions and entrapment of the Ag nanoparticles ensured that leakage of Ag ions was minimized. The coating showed biocompatibility with human osteoblasts, with a potential for bone implants, and at the same time complete inhibition of *E. coli* growth.

Subsequently, our group has also demonstrated that LBL coating of MTM/PDDA multilayers can be used to modify the surface of 3D inverted colloidal crystals hydrogel scaffolds which normally show poor cell attachment. Lee et al. demonstrated successful application of the multilayer to the cell culture constructs, which resulted in enhanced adhesion of Human thymic epithelial cells as opposed to a bare scaffold [81]. Most recently, Mehta et al. used PDDA/MTM films to modify the surface of PDMS to promote bone marrow cell attachment and spreading [82]. The authors utilized an automated microfluidic perfusion system to create multiple types of PEs coatings simultaneously in multiple channels based on LBL deposition of PDDA, MTM, type IV collagen, and fibronectin. They found that adherent primary bone marrow cells attached and spread best on a surface with composition of $(PDDA/MTM)_5$ $(Collagen/Fibronectin)_2$ with negatively charged fibronectin exposed on the top, remaining well spread and proliferating for at least 2 weeks. Compared to traditional more macroscopic LBL methods, this microfluidic nanocomposite process had advantages of greater flow control, automatic processing, multiplexed fabrication, and use of lesser amounts of polymers and protein solutions.

An interesting application of the MTM nanosheets was presented by Pappas et al. for engineering a neuronal interface for photoelectric stimulation of the cells [83]. The authors used multi-component LBL assemblies incorporating HgTe nanoparticles capped with PDDA/MTM film. The PDDA/MTM layer was used to improve biocompatibility and neuronal cell attachment, as well as a reservoir of Na^+ cations which were necessary for cell depolarization and firing of neurons. Other applications of LBL films for neural interfaces are given in the chapter on carbon nanotubes.

2.5. Anisotropic transport in clay multilayers

The stratified organizations of clay multilayers with respect to the substrate, the inorganic composition, and flat morphology of the platelets, have also imparted the clay multilayers with unique anisotropic transport properties. Kotov et al. realized the potential of the clay multilayers to preclude gas diffusion through defects and to design highly selective ultrathin membranes [65]. In their work, permeation rate of oxygen decreased 6.6 times for ~200-nm-thick PDDA/MTM film, while a permeation rate of aqueous vapors did not change at all. This effect was attributed to the dominance of solution/adsorption permeation mechanism over the Knudsen diffusion. This fact made the PE/MTM multilayers stand out among other thin films for which the diffusion through defects, was the primary mechanism of gas permeation. This finding also demonstrated both practical and fundamental importance of hybrid thin films that combined the properties of both organic and inorganic materials.

Jang et al. further showed that LBL films of MTM and cationic polyacrylamide could be grown on a polyethylene terephthalate (PET) film as a protective coating against diffusion of low molecular weight gasses [84]. After 30 clay/polymer layers were deposited, with a thickness of 571 nm, the resulting transparent film had an oxygen transmission rate (OTR) below the detection limit of commercial instrumentation (<0.005 cc/m^2/day/atm). This low OTR, which is unprecedented for a clay-filled polymer composite, is believed to be due to a brick wall nanostructure comprised of completely exfoliated clay in polymeric mortar (Fig. 8). The authors suggested that with an optical transparency greater than 90% and potential for microwaveability, this thin composite could be a good candidate for foil replacement in food packaging and may also

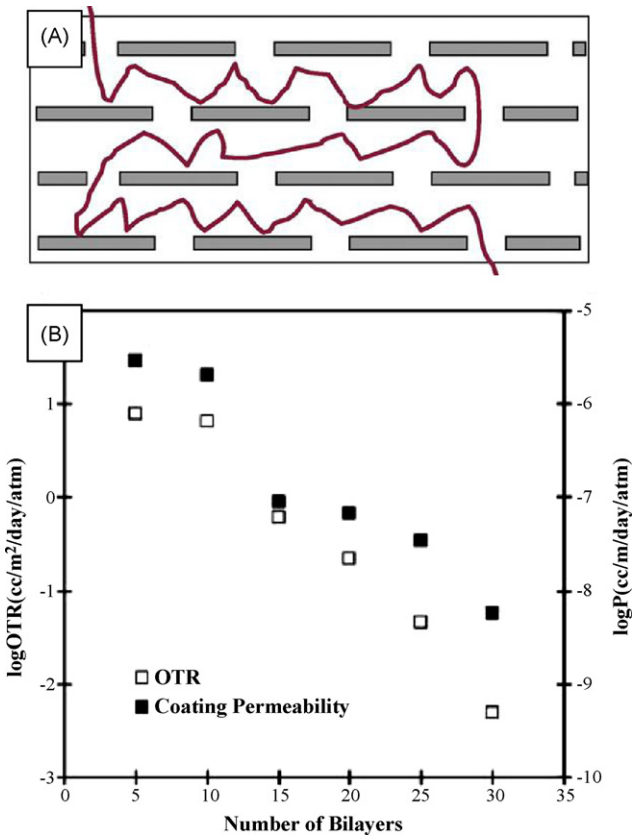

Fig. 8. (A) Schematic of the tortuous pathway for diffusion of gas molecules through clay LBL coating following a reflective tortuosity model proposed by Cussler. (B) Oxygen transmission rate and permeability as a function of the number of bilayers deposited. The OTR values are those of layer-by-layer thin films on a 179 μm PET substrate, while the permeability values are those of the thin films alone decoupled from the substrate (figure was reproduced from Ref. [84], with permission of the copyright holder).

be useful for flexible electronics packaging. Similarly, Ku et al. showed that 10 deposition cycles of poly(allylamine hydrochloride) (PAH)/PAA/PAH/saponite clay multilayer deposited on PET and following thermal cross-linking gave a 60% reduction in oxygen permeability when compared to pristine PET [85]. On the other hand, the authors noted that water permeability was not affected by cross-linking or the deposition cycles.

A new application for clay multilayers was also recently demonstrated, as coatings for fuel cells membranes. To demonstrate this, Kim et al. used saponite multilayers to enhance resistance to methanol diffusion through a Nafion membrane [86]. The authors used saponite in combination with ionic polyacetylenes (PEPy-C18) and they found that films composed of only 20 bilayers with a thickness of about 0.1 μm reduced the methanol permeability of the Nafion membrane to a half without deterioration of its in-plane proton conductivity.

The multilayers have also gathered attention with respect to lateral diffusion through the films, i.e. parallel to the orientation of adsorbed platelets. Westcott et al. have for example doped the PE/MTM coatings with corrosion inhibitors in order to utilize them as protective anti-corrosion coatings [87]. The resulting multilayers had superior corrosion protection when compared to hexavalent chromium coatings. In another example, Lutkenhaus et al. presented detailed characterization of anisotropic ionic conductivity in LBL assemblies of PEI, Laponite clay, and poly(ethylene oxide) [88]. This trilayer LBL structure was assembled using a combination of hydrogen bonding and electrostatic interactions. The authors have characterized the films using ellipsometry, profilometry, X-ray photon spectroscopy, AFM, SEM, wide angle XRD, grazing-incidence small-angle X-ray scattering, and electrochemical impedance spectroscopy. In the layered and anisotropic structure, they observed in-plane ion transport 100 times faster than cross-plane at 0% relative humidity.

2.6. Clay multilayers for optical and electronic applications

The stratified structure and well-defined, linear growth of the multilayers were also explored for incorporation of optically and electronically active molecules and polymers. With respect to incorporation of dye molecules, Laschewsky et al. synthesized an ionene-type polycation incorporating a nonlinear optical chromophore [89]. They employed it for LBL assembly with MTM nanosheets on charged and uncharged substrates. They monitored the assembly process by UV–vis spectroscopy and studied the influences of the choice of anionic species and of variations in the layer architecture. The authors observed different types of aggregation for different species of polyanions employed, and the increase of absorbance with the number of layers proved to be dependent on the specific multilayer composition. The degree of orientation of the chromophores was investigated by second-harmonic generation and the nonlinear response was found to depend strongly on the anionic species. This result demonstrated that PEs multilayers did not necessarily have a centrosymmetric structure, as generally assumed.

van Duffel et al. assembled fuzzy multi-compound films incorporating clay particles, PDDA, and methylene blue dye (MB+) and 4-[4-[*N*-allyl-*N*-methylamino]phenylazo]benzenesulfonic acid, sodium salt (NAMO−) [90]. The authors investigated glass/clay/PDDA/NAMO films by means of absorption spectroscopy, polarized absorption spectroscopy, and second-harmonic generation. They found that nonlinear optical properties of the films were determined by the adsorbed amount of NAMO and its noncentrosymmetric organization. These factors were in turn governed by the substrate type, the PDDA concentration, and the clay type. Optimized second-harmonic generation for the glass/Laponite/PDDA/NAMO films was found for composition in which the clay particles were deposited onto a (3-aminopropyl)-trimethoxysilane modified glass surface and PDDA chains were adsorbed from a 0.1 M solution.

Multilayers of hectorite clay were also used for preparation of functional films incorporating coumarin chromophore [91,92]. In these studies, the dye was intercalated in the clay platelets to form a negative clay/dye complex for LBL assembly with a polycation. The films were transparent with strong characteristic blue-green fluorescence.

Furthermore, Place et al. demonstrated preparation of LBL films by alternate deposition of clay particles and monomeric cyanine dye or poly-L-lysine with the same cyanine chromophore appended to it [93]. The authors showed that within the film structure the cyanine chromophore exhibits J-aggregate spectroscopic properties, either as the result of adsorption to the clay in the case of the monomeric dye or because it preexisted in this form in the case of the dye polymer. They also suggested that this composite assembly could potentially serve as a model for a light-harvesting photoantenna system. They demonstrated that capping the multilayer film with another layer of a different, cyanine dye, whose J-aggregate absorption band overlapped the fluorescence wavelength of the dye incorporated into the film, acted as an excitation energy donor. Efficient energy transfer was demonstrated for films containing no more than four dye layers for the monomeric donor dye or six layers for the polymeric donor dye.

Besides organic dyes, electrochemical and electrogenerated chemiluminescence of $Ru(bpy)_3^{2+}$ organometallic complex immobilized in $(clay/Ru(bpy)_3^{2+})_n$ multilayer films were investigated by

Guo et al. [94]. The stable multilayer films of clay and $Ru(bpy)_3^{2+}$ were assembled by alternate adsorption of negatively charged clay platelets and positively charged $Ru(bpy)_3^{2+}$ from their aqueous dispersions. UV–vis spectroscopy, QCM, CV, and electrogenerated chemiluminescence (ECL) were used to monitor the immobilization of $Ru(bpy)_3^{2+}$ and the regular growth of the $(clay/Ru(bpy)_3^{2+})_n$ multilayer films. The multilayer films modified electrode was used for the ECL detection of tripropylamine (TPA) and oxalate. The proposed novel, immobilized method exhibited good stability, reproducibility and high sensitivity for the determination of TPA and oxalate, which mainly resulted from the contributing of clay nanoparticles with appreciable surface area, special structural features, and unusual intercalation properties. Detection limits were 20 and 100 nM for TPA and oxalate, respectively, and the linear concentration range extended from 60 nM to 0.66 mM for TPA.

Optically active polymers have also been incorporated into clay multilayers. Lee et al., in their work on spin-assisted LBL assembly which we discussed in previous sections, incorporated poly(*p*-phenylene vinylene) (PPV) as an assembly component with Laponite [61]. The hybrid films were deposited using the electrostatic forces between the cationic PPV precursor and the negatively charged surface of layered silicate, and finally thermally converted to $(PPV/Laponite)_n$ film. The surface coverage of the PPV precursor onto layered silicate and vice versa was clearly observed using the contact angle measurement and surface dying technique. The continuous increase of UV–vis absorbance and PL intensity of the films with each bilayer demonstrated the regular and reproducible deposition of this system, and the Kiessig fringes and Bragg peaks in XRR spectra indicated the well-ordered internal structure.

In respect to electronic applications of clay multilayers, the main interest is once again in a potential for anisotropic conductivity due to layered structure and insulating properties of clay nanosheets. In this respect, Fan et al. prepared LBL films from MTM clay and a bicationic sexithiophene derivative (6TN) [95]. The main goal was to investigate the structure and layer ordering of these films suitable for future applications in organic semiconductor devices. The authors have compared the structure and morphology of 6TN/MTM multilayer thin films prepared in pure water and 0.1 M NaCl systems. The 6TN amphiphile showed unique aggregation behavior both in solution and on the surface, which changed with the presence of salts and a THF co-solvent. On clay surfaces, the 6TN aggregates deposited from saline solutions had a more uniform size distribution and surface coverage than that from a pure water system. This was verified by UV–vis spectra, XRD, and AFM.

2.7. 3D conformal coatings

An important opportunity for clay multilayers arises from the ability of LBL assemblies to form conformal coatings, which further expands the potential applications to 3D structures. Caruso et al. showed applicability of LBL technique to the formation of a range of polymer-core/inorganic-shell particles and inorganic hollow spheres (Fig. 9) [96,97]. The authors used titanium dioxide, silica, and Laponite nanoparticles as the inorganic building blocks for multilayer formation on polystyrene (PS) sphere templates. They studied influence of nanoparticle type, shape (spherical to sheet-like), and size (3–100 nm), and the diameter of the PS sphere templates (210–640 nm) on the formation of multilayer shells by transmission and scanning electron microscopy. They showed that the number of polyelectrolyte multilayers separating the nanoparticle layers, and the number of nanoparticle/polyelectrolyte deposition cycles could be varied to generate uniformly coated nanocomposite spheres. These hybrid core-shell particles were subsequently calcined to create well-defined hollow spheres with predetermined diameters. Such hollow spheres may find application in diverse areas, ranging from photonics to fillers and pigments to microencapsulation.

As we have mentioned in Section 2.4, Lee et al. also showed application of PDDA/MTM multilayer for preparation of conformal coatings on tissue engineering scaffolds constructed from 100 μm, interconnected pores [81]. The coating showed good stability in cell culture media and enhanced adhesion of human cells.

Finally, in a most recent study, Lu et al. demonstrated LBL assembly of 30–80 nm TiO_2 or SiO_2 nanoparticles and 50-nm diameter halloysite clay nanotubes on softwood fibers [98]. Using fluorescence and SEM microscopy, the authors showed complete nanoparticle coating on these fibers. The thickness of two-layer coating was estimated as 46, 58, and 115 nm for TiO_2, SiO_2, and halloysite tubules, respectively, which corresponded to ~1 wt.% nanoparticle loading on the fibers. The brightness test of paper handsheets prepared from nanocoated fibers showed that TiO_2 nanoparticle coating had handsheet reflectance of 84% at 450 nm, which was 4% higher than the brightness of the control sample from virgin fibers. The paper handsheets prepared with nanoparticle-coated fibers had 30–50% higher porosity with tensile strength index remaining close to the control sample.

3. LBL assemblies of carbon nanotubes

3.1. Structure and properties of CNTs

CNTs are rolled-up structures of a perfect hexagonal carbon crystal molecular sheet as a tubular cylinder. As the carbon crystal sheet, a graphene, is the strongest known material and a zero-band gap semiconductor, CNTs have shown many unique mechanical and electrical properties by the rolling direction types and the number of walls: single-walled and multi-walled carbon nanotubes (SWNTs, MWNTs). Stiffness and toughness of CNTs are arguably known as about up to 1 TPa and 300 GPa, respectively [99]. SWNTs are tough due to inward-collapse and plastic deformation [100], whereas MWNTs have shown unique 'sword-in-sheath' breakage pattern [99].

Electrically, a SWNT can be either semiconducting or metallic, which can be calculated by the chiral vecter indices (n, m) of graphene layer [101]. Although separation of each type and production techniques of one structural kind are actively under development, overall one-third of bulk SWNTs are metallic and the rest are semiconducting. Besides the properties of each CNT, the type distribution of CNTs collectively affects the macro-scale performance of composites. Thus, the identification of CNT type as well as controlling the distribution ratio is critical research factors for the assembly of CNT multilayers. Raman spectroscopy is widely used to extract the information of individual CNT structures and types [102,103]. Furthermore, theoretical predictions of each type of CNTs were well documented for such as electronic, photonic and phonon dispersion states in a single CNT [101,104,105] (Fig. 10). Usually, the length of CNTs varies in μm to cm ranges so that the extremely high aspect ratios of CNTs in nano-scale dimensions further enrich the application potentials. However, given the hydrophobic graphene and smooth crystalline walls, dispersion of CNTs still remains as grand challenges. Collective van der Waals forces, which exert in a CNT bundle and prevent exfoliation, dramatically increase as the length increases. Thus, currently only limited lengths under 100 μm long CNTs are employed as solution processing of CNT, which is the pre-requirement of LBL assemblies. Furthermore, two typical dispersion techniques of CNTs, which are oxidation of CNTs and interfacing with stabilizers, severely degrade, or at least modify, the properties of CNTs. Overall, tipping point of LBL assembly of CNTs originated from the widespread difficulties of uniform dispersion as well as precise controlled structural cast-

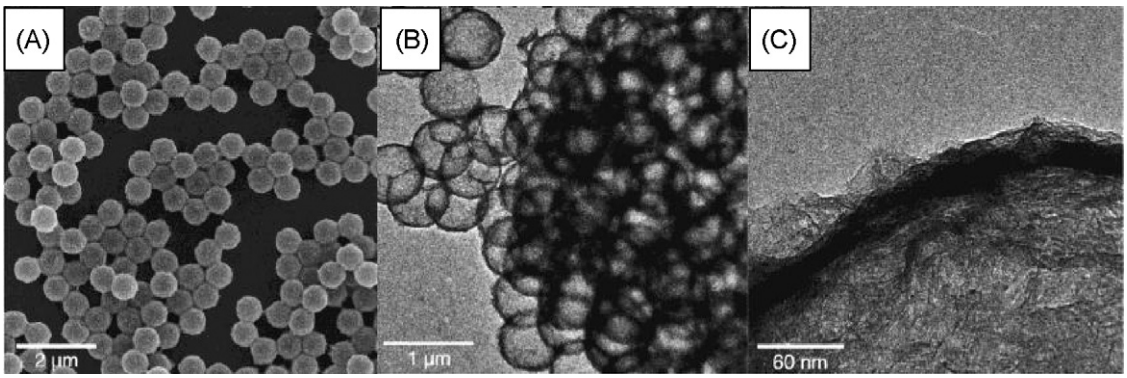

Fig. 9. SEM (A) and TEM (B and C) images of hollow Laponite spheres obtained after calcination of PS spheres (640 nm) coated with five Laponite nanoparticle/PDADMAC multilayers (figure was reproduced from Ref. [97], with permission of the copyright holder).

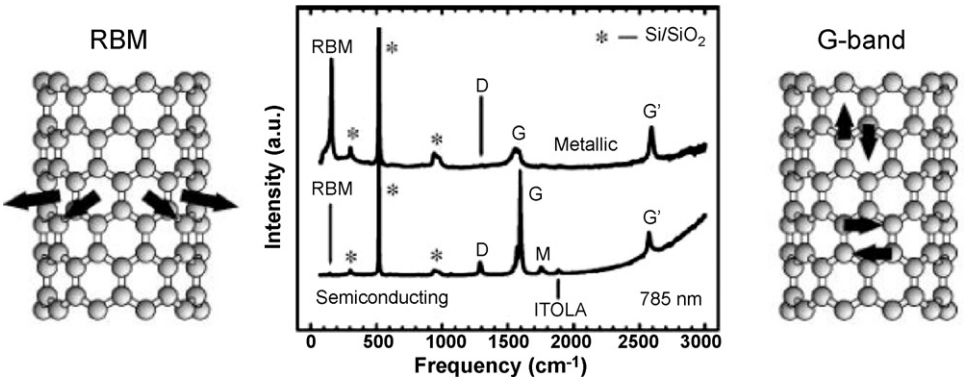

Fig. 10. Representative image of Raman spectroscopy measurements. Left shows the radial breathing mode (RBM) and right depict the graphene corresponding band (G-band). Middle top and bottom spectrograms indicate the metallic and the semiconducting SWNTs, respectively (figure was reproduced from Ref. [101], with permission of the copyright holder).

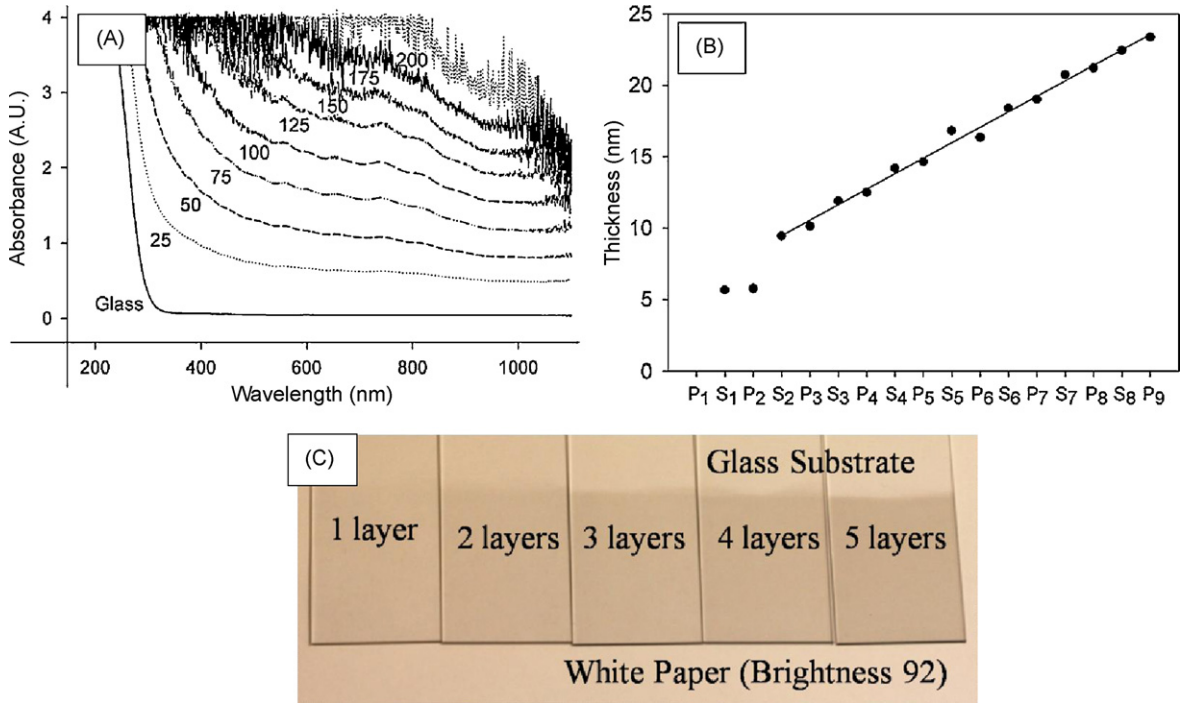

Fig. 11. Typical LBL layering process of SWNTs monitored by (A) UV–vis light absorbance spectroscopy and (B) thickness estimation by ellipsometry. (C) Optical transparency changes by adding SWNT layers. The bumpy peaks in a spectrogram of (A) indicate van Hove singularities of SWNTs, which are indirect evidence of good exfoliation as well as dispersion (figure was reproduced from Ref. [106], with permission of the copyright holder).

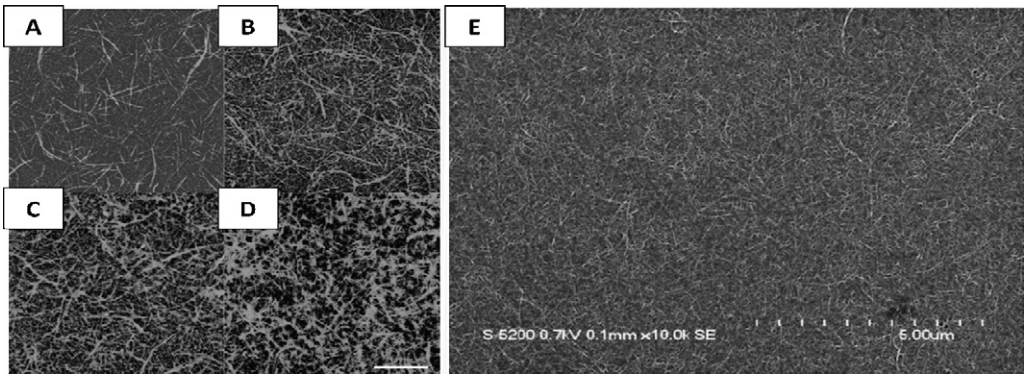

Fig. 12. Typical microscopic images of CNT LBL assembly. (A–D) Tapping-mode AFM images of (A) 1, (B) 3, (C) 6, and (D) 9 layers of [PDDA/SWNT] LBL. The scale bar and *z*-heights represent 1.25 μm and 50 nm, respectively. (E) SEM images of 9 layers of [PDDA/SWNT] LBL film (figure was reproduced from Ref. [107], with permission of the copyright holder).

ing into a solid composite by conventional composite processing techniques.

3.2. Structural organization in multilayers of carbon nanotubes

The primary advantages of LBL assembly of CNTs include (1) uniform dispersion of CNTs into a composite which is enabled by direct adsorption of CNTs from a solution to a solid state without phase segregation, (2) tunable multi-functional properties of a composite which is enabled by accurately controlled multi-component nanolayers, and (3) simple, robust, and versatile processibility of CNT nano-thin composite coating. The early pioneering work of CNT LBL assembly is the introduction of successful conquest over dispersion challenges of CNTs in polymer composites. Mamedov et al. [8] reported that exceptionally uniform dispersion of SWNTs in nano-thin layered structures showed great potential in their mechanical properties even with weak polymers, which has drawn broad attention from various disciplines. Notable mechanical functionalities of the SWNT LBL composite are originated by not just uniform dispersion, but also high loading of CNTs and functionally activated interfacial bonding between CNTs and polyelectrolyte matrix, poly(ethylene imine) (PEI). Successive experimental reports confirmed that LBL assembly of SWNTs indeed allowed exceptional exfoliation and homogeneous dispersion in a polymeric composite [107] and nano-scale stepwise deposition of CNTs showed tremendous potential promise for development of a wide range of functional materials [108–111] (Figs. 11 and 12). The loading of CNTs in LBL assembled composites can be controlled in the range of 10% [106] to 75% [112], which depends on many variables of LBL assembly such as LBL polymer matrix, stabilizer of CNTs, process conditions, and so forth. The layered growth by dipping is usually linear with constant slope [113,114] and the surface roughness of each layers rely on the layer growth rate and the thickness of each layer [114] although it is limited within nano-scale ranges, which allow precise organization controls during CNT LBL assembly. The adsorption interaction between CNTs and polymers can be either conventional electrostatic force [115], hydrogen bonds [113], or van der Waals interactions [116] and later modified to strong covalent bonds [113]. The features of LBL assembly were also effective to various sizes of carbon nanomaterials including MWNTs [108], vapor grown hollow carbon fibers with diameter size of 50–150 nm [117], and exfoliated graphene nanoplatelets [118].

The unusual properties of CNTs are modulated in LBL assembled nanocomposites by mix-matching with complementary polymeric LBL partners. For their uses as sensors, cell scaffolds, drug delivery carrier, and fuel cell membranes, the judicial selection of polymeric matrix in LBL assembly is required for enhancing the performances in the field of application. The scopes of macromolecules as CNTs' LBL counter partner are extended from conventional LBL polymers such as poly(vinyl alcohol) (PVA) [106], poly(allylamine hydrocholoride) (PAH) [119], poly(ethylene imine) (PEI) [8,120], poly(diallyldimethyl ammonium choloride) (PDDA), poly(acrylic acid) (PAA) [121], to functional materials like poly(3,4-ethylenedioxythiphene)/poly(styrene sulfonate) (PEDOT/PSS) [122], poly(anilne) (PANI) [123], polypyrrole (PPy) [124,125], light sensitive diazoresin (DR) [113], poly(viologen) derivatives [126,127], porphyrin [127], prussian blue (PB) [128,129], and to bio related materials such as blood-compatible poly(lactic acid-co-glycolic acid) (PLGA) [130], biopolymer Chitosan [129], antimicrobial lysozyme (LSZ) [131], antisense oligodeoxynucleotide (ASODN) enzymes [132]. In the following subsections, detailed examples of CNT LBL assembly classified by applications are introduced.

3.3. Electrical conductor applications

The combination of exceptional nano-organization of LBL assembly and unique electrical properties of CNTs has opened wide research opportunities. In 2005, Kovtyukhova et al. reported that LBL composites of densely distributed SWNTs have highly anisotropic electrical properties because of layered structures [109]. The conductivity differences between in-plane and out-of-plane directions are more than factor of three so that great potential to property modulation was suggested with ultrathin film thickness controls [109,133]. The same research team further demonstrated p–n hetero junction diodes on Au nanowires with high rectifying efficiency, which was fabricated by mixed LBL assembly of SWNTs, conductive polymer (PANI), and semiconducting nanoparticles on Au nanowires [110]. In this research, the features of SWNT LBL films were highly p-type conductive and ultrathin coating over Au nanowires, and stable to provide junction performances even after dissolution of alumina membranes. The test schematics and performances are shown in Fig. 13. As a way to improve the electrical properties of LBL assembled CNT nanocomposites, Shim et al. reported that electrical conductivities were depended on micro-/nano-scale continuous conductive path by the analysis specific to molecular structures of LBL composites [106]. Following this analysis, heat treatment techniques at 200 and 300 °C were suggested to form tighter SWNT connections whose in situ measurements of nano-structural changes during the treatments were demonstrated. These treatments improved the electrical conductivities of SWNT LBL film by two orders of magnitude. Furthermore, they revealed that LBL assembled SWNT composites were up to 10 times stronger than SWNT-only mats. The films were suggested to be used as high-performance transparent conductors (TCs), which justified the advantages of SWNT

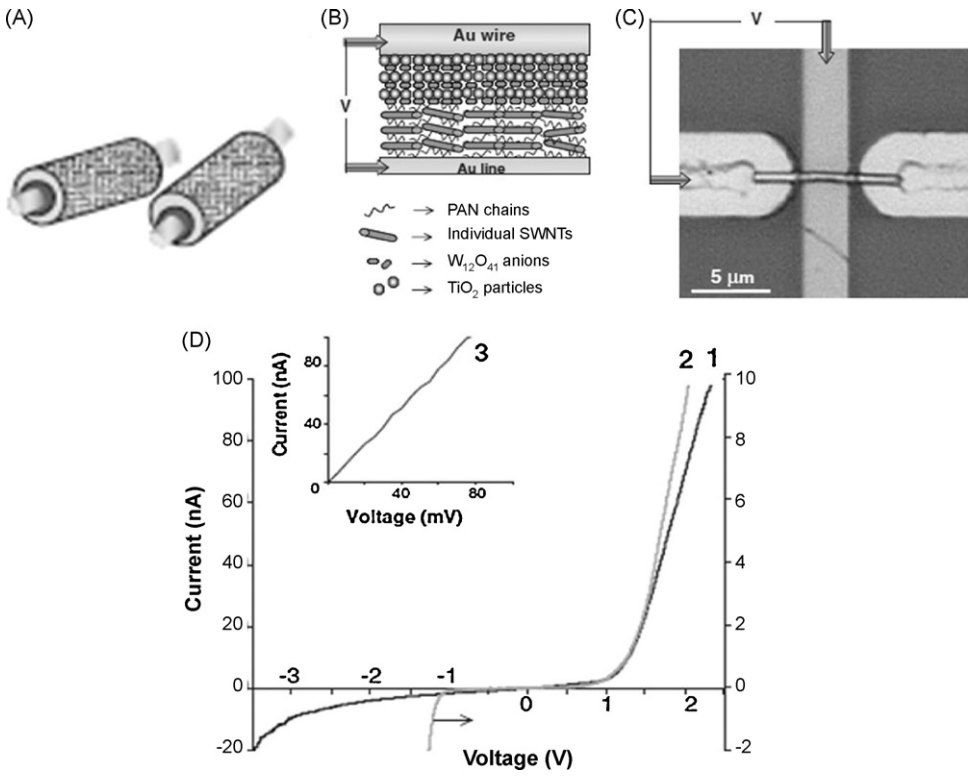

Fig. 13. Tube-shell type p–n junction LBL on a Au nanowire. Top showed schematic models of (A) tube-shell p–n junction, (B) structural p–n junction layers, and (C) microscope image of test setup. SWNT LBL thin film provide p-type conductor. (D) *I–V* characteristics of (1) p- and n-type layer coating, (2) n-type only coating, and (3) p-type only coating on a Au nanowire (figure was reproduced from Ref. [110], with permission of the copyright holder).

LBL composites as new class electronic materials [106] (Fig. 11C). These high electrical properties of SWNT LBL films were further demonstrated as low cost, high efficient polymeric thin film transistor (TFT) by Xue et al. [134] (Fig. 14). The same team further suggested that these micro-patterned electronic devices could be fabricated on a highly flexible substrate by LBL assembly [135].

Among the applications of these properties, TCs provide direct commercialization opportunities utilizing precise nano-scale organization of LBL assembly of SWNTs. Yu et al. reported a SWNT/PDDA LBL composite with 2.5 kΩ/sq at 86.5% light transmittance [136] and they further formed the similar LBL coating as a transparent surface electrode on a PVDF actuator whose audio speaker performances were demonstrated as excellent [137]. Ham et al. utilized conductive PEDOT/PSS with SWNTs to form TCs by LBL assembly [122] although the TC performances are lower than SWNT-only mats, Bucky papers. The competitive TC performances of SWNT LBL composites compared to conventional ITOs were reported by Shim et al., whose TC coating with vigorous acid doping demonstrated lower than 100 Ω/sq at 80% light transmittance. Unlike other processes for SWNT nanomats – bucky papers, simple and easy to scale-up processibilty of LBL assembly and the high mechanical integrity of SWNT LBL composites make them to be a viable alternative option of TC materials of choice. As extension of TC properties, Jain et al. reported that durable electrochromic devices, which usually require high transparency, high contrast, low surface roughness, accurate thickness control, and fast ion conductivity, were fabricated by LBL assembly of poly[2-(3-thienyl)ethoxy-4-butylsulfonate]/poly(allylamine hydrochloride) on SWNT electrodes [138].

3.4. Sensor applications

A great deal of SWNT nanocomposites fabricated by LBL assembly technique were applied to physical/chemical sensors by utilizing (1) electrical property change of CNTs by chemical species,

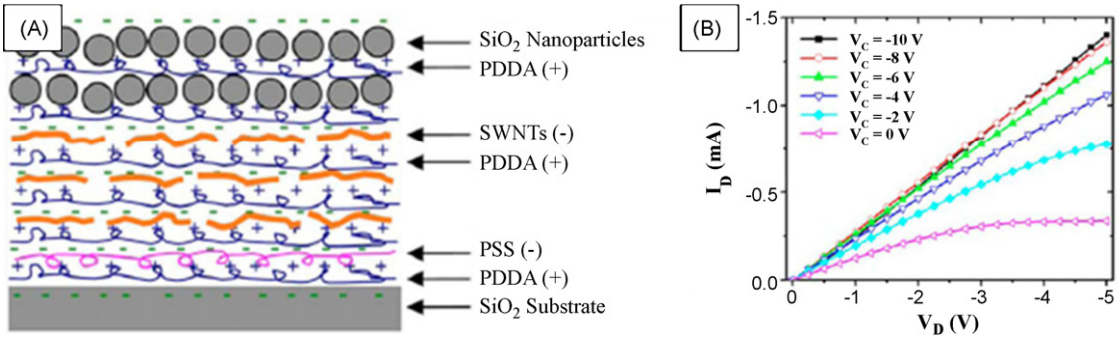

Fig. 14. (A) Schematic presentation of molecular assembly structure of TFT with SWNT semiconducting layers and SiO_2 nanoparticle dielectric layers. (B) Examples of TFT performances which showed drain current–voltage characteristics by varying the gate voltage from −10 to 0 V (figure was reproduced from Ref. [134], with permission of the copyright holder).

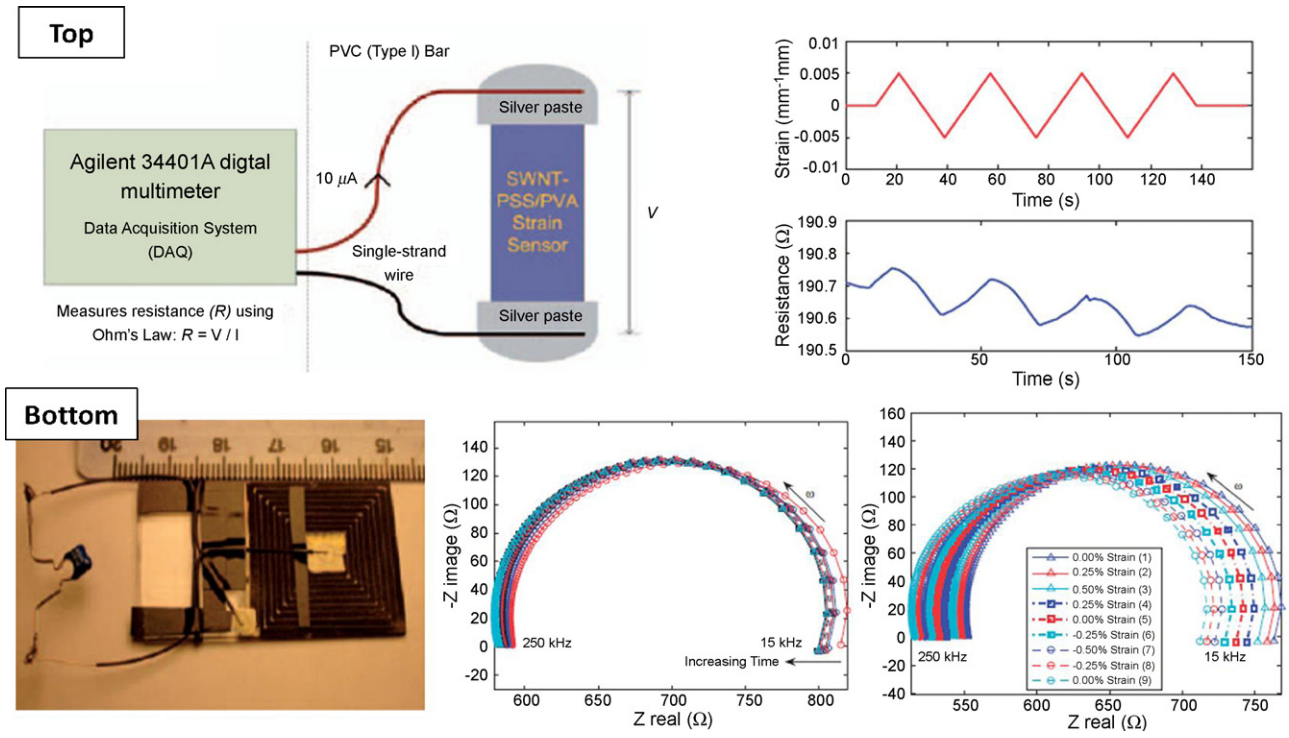

Fig. 15. (Top) Strain-sensor application of SWNT LBL films. (Bottom) Patterned SWNT LBL films as an inductively coupled antenna used in a RFID system and their sensor performances (figure was reproduced from Ref. [139], with permission of the copyright holder).

(2) electrochemical responses of counter LBL partner of CNTs, (3) structural deformation induced electrical resistance changes of a composite, or (4) specially designed micro-/nano-electrical mechanical system (MEMS/NEMS) devices. Typical examples of monitoring physical and chemical states by CNT LBL composites are demonstrated by Loh et al. (Fig. 15). They reported that a strain sensor by tailored piezoresistive response [139] and a pH sensing strip sensitive enough to monitor environment changes caused by corrosion of metal structures [123] were constructed by SWNT/PVA and SWNT/PANI LBL composites, respectively. Detection targets of SWNT LBL composites are only limited by our imagination. Biological materials such as DNA [140], glucose [124,125,129,141–146], dopamine [147,148], uric acid [147], and toxic materials such as arsenic [149], phenols [125] were often detected by amperometric measurements of CNT LBL nanocomposites utilizing the combinations of electrocatalytic activities, electrochemical sensitivities of CNTs, and various materials immobilization given by versatile selections of LBL assembly. Environmental changes like humidity are easily monitored by CNT LBL composites [150].

The integration of LBL assembled composites into MEMS/NEMS devices are new fusion technology of top-down and bottom-up nano-process [66]. CNTs are also leading these frontiers owing to their unique electrical and mechanical properties. The LBL assembled SWNT nanocomposites were patterned as flexible micro-cantilever arrays whose movements were demonstrated by Xue et al. [151]. This CNT LBL micro-cantilever can find future applications in biosensors and micro-valve for microfluidic structure channels. As another recent important progress, highly efficient nanomembrane micro-sensor platforms by MEMS devices were developed by SWNT LBL composites [152] following ultrathin membrane design concepts [153]. The thickness of freely suspended sensors could be varied from 7 to 26 nm due to strong mechanical properties of SWNT LBL composites. Kang et al. claims that this freely suspended nanomembrane array open a breakthrough path to new nanomembrane micro-sensors by exceptional sensitivity, versatile multi-component functionality, and extreme stability [152] (Fig. 16).

3.5. Fuel cell applications

Combined with unique merit of LBL assemblies such as nano-thin orgarnized structures, controlled porosity, and free selection of ionic matrix, fuel cell proton exchange membranes (PEMs) were constructed by LBL assembled CNT nanocomposites as highly conductive and chemically durable electrodes [135,154–156]. Michel et al. reported that CNTs wrapped with Nafion and Pt catalysts showed unusual fuel cell performances when they are LBL assembled to a fuel cell PEM, which is featured with nano-scale optimized electron/proton movements, simple, low cost production, and efficient utilization of Pt catalysts as well as with mechanical strength, high electrical, high thermal conductivities, and stable chemical durability [154]. This LBL scheme is further adapted as blending techniques between proton exchange Nafion and CNTs to nano-layer controlled structures, whose aim is to improve proton conduction efficiency at high operating temperature [157]. Interestingly, biofuel cell applications were also developed by CNT/poly-L-(lysine)/fungal laccase LBL assembly, which features electrical potential generation by stable enzyme immobilization [158].

3.6. Nano-/micro-shell LBL coatings and biomedical applications

The LBL assembly principles are effective not only on bulk planar surfaces but also on micro-/nano-complex objects which may have potential applications such as in biomedicine and biocompatible micro-prosthetic devices. For these complex coatings, two design schemes associated with CNTs are introduced. The first is assembling CNT LBL films over microspheres. Starting from Sano et al.'s initial success reports of preparing hollow carbon micro-vessels in 2002 [159], the efforts have been directed at improving the properties of micro-spherical shells such as strength, permeability, and

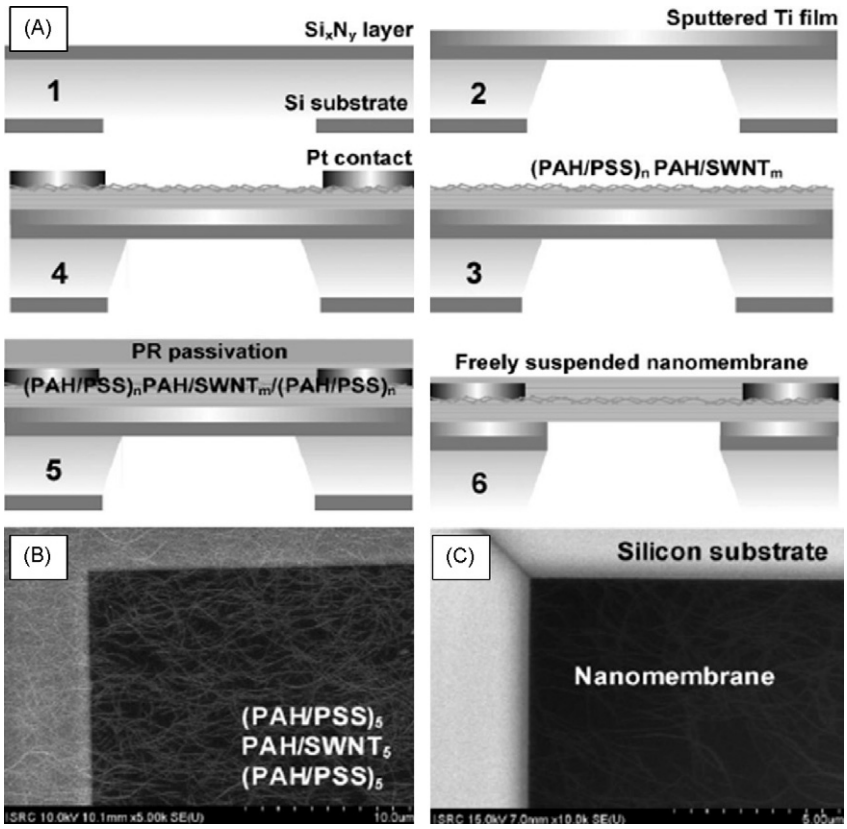

Fig. 16. (A) Fabrication process of SWNT LBL nanomembrane arrays. (B) Top view and (C) bottom view of SEM images of MEMS structure integrated nanomembranes (figure was reproduced from Ref. [152], with permission of the copyright holder).

porosity [160,161], and to modify production process by changing types of microsphere templates [160,162] or by adding calcination process to remove polymers [161]. Various types of micro-objects by desires can be used as templates for LBL assemblies. Coating over soft-microcapsules was developed to protect liposome by CNT-reinforced LBL composites [119]. Pan et al. reported that electrospun polystyrene (PS) microfibers were employed as a template of MWNT LBL composites [163]. By dissolving of PS, hollow microtubular structures of MWNT LBL nanocompsites were obtained easily.

The other types of nanoshell designs are direct LBL assemblies over CNT strands-like templates. Artyukhin et al. reported that SWNTs attached with ionic pyrene derivatives were successfully wrapped by polymeric LBL assemblies [164]. This technique has been further applied to produce porous indium oxide nanotubes which may be useful as toxic gas detectors [165]. Du et al. reported that nano-tubular structures of indium oxide produced by LBL assembly over CNT strands and purified by calcinations greatly expanded their active surface areas and simultaneously improved sensitivity to NH_3 gas [165]. As other examples, stable biomolecule coatings over MWNTs were demonstrated by Liu et al. [166]. They formed a thick and molecular brick like rigid β-cyclodextrin layers over a MWNT by LBL assembly techniques. Certainly, this biomolecule wrapping of CNTs was proved to be effective tools to intracellular delivery of biomedicine [132]. Jia et al., reported that anti-cancer enzymes, ASODNs, and fluorescent labeling quantum dots coated on MWNTs by LBL assembly were successfully injected into tumor cells [132]. Thus, further developments of LBL assembly over CNT nano-objects may be needed for the future biomedicine or tissue engineering application.

Along with above structural controls, biomedical functionality and cell interface compatibility tests were performed with CNT LBL nanocomposites. Following cellular adhesion experiments [167], Gheith et al. reported that neuronal cells and their neurite growth were enhanced by electrical stimulus through CNT LBL composites [121], which was the first observation of cellular interactions to CNT materials by electrical potential. Furthermore, these neural cell tests were extended to the differentiation of embryonic neural stem cells on CNT LBL nanocomposites [120]. These live cell interface experiments corroborate that CNT LBL composites are indeed one of the most viable functional materials options for biomedical implant, prosthetic devices, and stem cell growth platforms.

Another type of biocompatible, blood-compatible surface tests were performed on LBL assembled CNT/PLGA nanocomposites for the aim of thromboresistance suppression to foreign artificial blood prostheses [130]. In contrast to this biocompatible surface, antifouling or antimicrobial coating provides also good application examples of LBL assembly. Nepal et al. designed LBL assembly of antimicrobial lysozyme (LSZ) with CNTs for the aim of improving mechanical properties of surfaces [131]. The nanoindentation measurement used there, however, needs to be carefully analyzed to determine the Young's modulus and hardness of LBL film, because the substrate effect is so significant in a thin film. The suggestion of valid measurement condition is no deeper than 10% of total thickness as indicated by Pavoor et al. [168].

4. Conclusions

LBL technology offers an interesting possibility to control the structure of composite materials at nanometer scale with high degree of accuracy. This is the pathway to attaining the record properties of materials and some of them were demonstrated already. This fact has fundamental significance because it allows one to establish the design rules for composite structures initially in the small scale and then to replicate them in a larger scale proba-

bly with other methods of composite manufacturing. Some of the future challenges that we see in this field include the following: (1) scale up of the LBL materials and development of new methods of deposition, which combine both high degree of the structural control and the speed. Substantial effort in this direction is being already undertaken. (2) Realization of greater mechanical properties in CNT composites. Currently, the ideal stress transfer was only realized for clay platelets. CNTs will require much greater research effort to achieve such conditions. This challenge will probably imply a substantial change in understanding how the deformations should be transferred through different interfaces. (3) Wider utilization of the properties of the described composites in the biological arena. Currently we are just in the beginning of development of a new generation of composite biomaterials made by LBL technique that are likely to provide enabling technologies to many applications in medicine from implants to imaging.

Acknowledgments

PP thanks the Fannie and John Hertz Foundation for support of his work through a graduate fellowship. PP also acknowledges his current support through Willard Frank Libby Postdoctoral Fellowship at Argonne National Laboratories under a DOE contract DE-AC02-06CH11357.

References

[1] D.V. Talapin, ACS Nano 2 (2008) 1097.
[2] R.K. Iler, J. Colloid Interface Sci. 21 (1966) 569.
[3] G. Decher, J. Schmitt, Prog. Colloid Polym. Sci. S 89 (1992) 160.
[4] G. Decher, Science 277 (1997) 1232.
[5] P.T. Hammond, Adv. Mater. 16 (2004) 1271.
[6] D. Ingersoll, P.J. Kulesza, L.R. Faulkner, J. Electrochem. Soc. 141 (1994) 140.
[7] N.A. Kotov, I. Dekany, J.H. Fendler, J. Phys. Chem. 99 (1995) 13065.
[8] A.A. Mamedov, N.A. Kotov, M. Prato, D.M. Guldi, J.P. Wicksted, A. Hirsch, Nat. Mater. 1 (2002) 190.
[9] C.Y. Jiang, H.Y. Ko, V.V. Tsukruk, Adv. Mater. 17 (2005) 2127.
[10] S.W. Keller, H.N. Kim, T.E. Mallouk, J. Am. Chem. Soc. 116 (1994) 8817.
[11] T.M. Cooper, A.L. Campbell, R.L. Crane, Langmuir 11 (1995) 2713.
[12] P. Podsiadlo, S.Y. Choi, B. Shim, J. Lee, M. Cuddihy, N.A. Kotov, Biomacromolecules 6 (2005) 2914.
[13] P. Podsiadlo, L. Sui, Y. Elkasabi, P. Burgardt, J. Lee, A. Miryala, W. Kusumaatmaja, M.R. Carman, M. Shtein, J. Kieffer, J. Lahann, N.A. Kotov, Langmuir 33 (2007) 7901.
[14] J.A. He, R. Valluzzi, K. Yang, T. Dolukhanyan, C.M. Sung, J. Kumar, S.K. Tripathy, L. Samuelson, L. Balogh, D.A. Tomalia, Chem. Mater. 11 (1999) 3268.
[15] K. Araki, M.J. Wagner, M.S. Wrighton, Langmuir 12 (1996) 5393.
[16] Y. Lvov, M. Onda, K. Ariga, T. Kunitake, J. Biomater. Sci.-Polym. Ed. 9 (1998) 345.
[17] L. Richert, P. Lavalle, D. Vautier, B. Senger, J.F. Stoltz, P. Schaaf, J.C. Voegel, C. Picart, Biomacromolecules 3 (2002) 1170.
[18] F. Boulmedais, V. Ball, P. Schwinte, B. Frisch, P. Schaaf, J.C. Voegel, Langmuir 19 (2003) 440.
[19] Y. Lvov, G. Decher, G. Sukhorukov, Macromolecules 26 (1993) 5396.
[20] J.D. Hong, K. Lowack, J. Schmitt, G. Decher, Prog. Colloid Polym. Sci. 93 (1993) 98.
[21] Y. Lvov, K. Ariga, T. Kunitake, Chem. Lett. (1994) 2323.
[22] P.J. Yoo, K.T. Nam, J.F. Qi, S.K. Lee, J. Park, A.M. Belcher, P.T. Hammond, Nat. Mater. 5 (2006) 234.
[23] Z.Y. Tang, Y. Wang, P. Podsiadlo, N.A. Kotov, Adv. Mater. 18 (2006) 3203.
[24] L. Zhai, F.C. Cebeci, R.E. Cohen, M.F. Rubner, Nano Lett. 4 (2004) 1349.
[25] L. Zhai, M.C. Berg, F.C. Cebeci, Y. Kim, J.M. Milwid, M.F. Rubner, R.E. Cohen, Nano Lett. 6 (2006) 1213.
[26] D.L. Ellis, M.R. Zakin, L.S. Bernstein, M.F. Rubner, Anal. Chem. 68 (1996) 817.
[27] C.A. Constantine, S.V. Mello, A. Dupont, X.H. Cao, D. Santos, O.N. Oliveira, F.T. Strixino, E.C. Pereira, T.C. Cheng, J.J. Defrank, R.M. Leblanc, J. Am. Chem. Soc. 125 (2003) 1805.
[28] D.S. Koktysh, X.R. Liang, B.G. Yun, I. Pastoriza-Santos, R.L. Matts, M. Giersig, C. Serra-Rodriguez, L.M. Liz-Marzan, N.A. Kotov, Adv. Funct. Mater. 12 (2002) 255.
[29] K.C. Wood, H.F. Chuang, R.D. Batten, D.M. Lynn, P.T. Hammond, Proc. Natl. Acad. Sci. U.S.A. 103 (2006) 10207.
[30] C.M. Jewell, J.T. Zhang, N.J. Fredin, D.M. Lynn, J. Control. Release 106 (2005) 214.
[31] J.S. Lee, J. Cho, C. Lee, I. Kim, J. Park, Y.M. Kim, H. Shin, J. Lee, F. Caruso, Nat. Nanotechnol. 2 (2007) 790.
[32] J. Hiller, J.D. Mendelsohn, M.F. Rubner, Nat. Mater. 1 (2002) 59.
[33] D.M. DeLongchamp, P.T. Hammond, Adv. Funct. Mater. 14 (2004) 224.
[34] I. Moriguchi, J.H. Fendler, Chem. Mater. 10 (1998) 2205.
[35] R. Heuberger, G. Sukhorukov, J. Voros, M. Textor, H. Mohwald, Adv. Funct. Mater. 15 (2005) 357.
[36] H. Tokuhisa, P.T. Hammond, Adv. Funct. Mater. 13 (2003) 831.
[37] J. Zhang, B. Senger, D. Vautier, C. Picart, P. Schaaf, J.C. Voegel, P. Lavalle, Biomaterials 26 (2005) 3353.
[38] A.A. Mamedov, A. Belov, M. Giersig, N.N. Mamedova, N.A. Kotov, J. Am. Chem. Soc. 123 (2001) 7738.
[39] D.Y. Wang, A.L. Rogach, F. Caruso, Nano Lett. 2 (2002) 857.
[40] J.Y. Liu, L. Cheng, Y.H. Song, B.F. Liu, S.J. Dong, Langmuir 17 (2001) 6747.
[41] Y. Shen, J.Y. Liu, J.G. Jiang, B.F. Liu, S.J. Dong, J. Phys. Chem. B 107 (2003) 9744.
[42] A.J. Nolte, M.F. Rubner, R.E. Cohen, Langmuir 20 (2004) 3304.
[43] A.A. Mamedov, N.A. Kotov, Langmuir 16 (2000) 5530.
[44] O.L. Manevitch, G.C. Rutledge, J. Phys. Chem. B 108 (2004) 1428.
[45] R.H.A. Ras, Y. Umemura, C.T. Johnston, A. Yamagishi, R.A. Schoonheydt, Phys. Chem. Chem. Phys. 9 (2007) 918.
[46] E.R. Kleinfeld, G.S. Ferguson, Science 265 (1994) 370.
[47] G.S. Ferguson, E.R. Kleinfeld, Adv. Mater. 7 (1995) 414.
[48] Y. Lvov, K. Ariga, I. Ichinose, T. Kunitake, Langmuir 12 (1996) 3038.
[49] K. Ariga, Y. Lvov, I. Ichinose, T. Kunitake, Appl. Clay Sci. 15 (1999) 137.
[50] N.A. Kotov, T. Haraszti, L. Turi, G. Zavala, R.E. Geer, I. Dekany, J.H. Fendler, J. Am. Chem. Soc. 119 (1997) 6821.
[51] B. van Duffel, R.A. Schoonheydt, C.P.M. Grim, F.C. De Schryver, Langmuir 15 (1999) 7520.
[52] K. Glinel, A. Moussa, A.M. Jonas, A. Laschewsky, Langmuir 18 (2002) 1408.
[53] P.Y. Vuillaume, A.M. Jonas, A. Laschewsky, Macromolecules 35 (2002) 5004.
[54] P.Y. Vuillaume, K. Glinel, A.M. Jonas, A. Laschewsky, Chem. Mater. 15 (2003) 3625.
[55] J.H. Rouse, G.S. Ferguson, Clay Clay Miner. 55 (2007) 160.
[56] L. Li, R.Z. Ma, Y. Ebina, N. Iyi, T. Sasaki, Chem. Mater. 17 (2005) 4386.
[57] Z.P. Liu, R.Z. Ma, M. Osada, N. Iyi, Y. Ebina, K. Takada, T. Sasaki, J. Am. Chem. Soc. 128 (2006) 4872.
[58] M. Szekeres, A. Szechenyi, K. Stepan, T. Haraszti, I. Dekany, Colloid Polym. Sci. 283 (2005) 937.
[59] J. Bin Han, J. Lu, M. Wei, Z.L. Wang, X. Duan, Chem. Commun. 41 (2008) 5188.
[60] O. Altuntasoglu, U. Unal, S. Ida, M. Goto, Y. Matsumoto, J. Solid State Chem. 181 (2008) 3257.
[61] H.C. Lee, T.W. Lee, T.H. Kim, O.O. Park, Thin Solid Films 458 (2004) 9.
[62] P. Podsiadlo, M. Michel, J. Lee, E. Verploegen, N.W.S. Kam, V. Ball, Y. Qi, A.J. Hart, P.T. Hammond, N.A. Kotov, Nano Lett. 8 (2008) 1762.
[63] C. Picart, J. Mutterer, L. Richert, Y. Luo, G.D. Prestwich, P. Schaaf, J.C. Voegel, P. Lavalle, Proc. Natl. Acad. Sci. U.S.A. 99 (2002) 12531.
[64] E.P. Giannelis, Adv. Mater. 8 (1996) 29.
[65] N.A. Kotov, S. Magonov, E. Tropsha, Chem. Mater. 10 (1998) 886.
[66] F. Hua, T.H. Cui, Y.M. Lvov, Nano Lett. 4 (2004) 823.
[67] X.W. Fan, M.K. Park, C.J. Xia, R. Advincula, J. Mater. Res. 17 (2002) 1622.
[68] Z.Y. Tang, N.A. Kotov, S. Magonov, B. Ozturk, Nat. Mater. 2 (2003) 413.
[69] P. Podsiadlo, Z.Y. Tang, B.S. Shim, N.A. Kotov, Nano Lett. 7 (2007) 1224.
[70] J.H. Waite, M.L. Tanzer, Science 212 (1981) 1038.
[71] P. Podsiadlo, Z.Q. Liu, D. Paterson, P.B. Messersmith, N.A. Kotov, Adv. Mater. 19 (2007) 949.
[72] P. Podsiadlo, A.K. Kaushik, E.M. Arruda, A.M. Waas, B.S. Shim, J.D. Xu, H. Nandivada, B.G. Pumplin, J. Lahann, A. Ramamoorthy, N.A. Kotov, Science 318 (2007) 80.
[73] P. Podsiadlo, A.K. Kaushik, B.S. Shim, A. Agarwal, Z.Y. Tang, A.M. Waas, E.M. Arruda, N.A. Kotov, J. Phys. Chem. B 112 (2008) 14359.
[74] V. Vertlib, M. Dietiker, M. Plotze, L. Yezek, R. Spolenak, A.M. Puzrin, J. Mater. Res. 23 (2008) 1026.
[75] Y. Lvov, K. Ariga, I. Ichinose, T. Kunitake, J. Am. Chem. Soc. 117 (1995) 6117.
[76] Y.M. Lvov, G.B. Sukhorukov, Biol. Membr. 14 (1997) 229.
[77] Y.L. Zhou, Z. Li, N.F. Hu, Y.H. Zeng, J.F. Rusling, Langmuir 18 (2002) 8573.
[78] Z. Li, N.F. Hu, J. Electroanal. Chem. 558 (2003) 155.
[79] E. Lojou, P. Bianco, Electroanalysis 18 (2006) 2426.
[80] P. Podsiadlo, S. Paternel, J.M. Rouillard, Z.F. Zhang, J. Lee, J.W. Lee, L. Gulari, N.A. Kotov, Langmuir 21 (2005) 11915.
[81] J. Lee, S. Shanbhag, N.A. Kotov, J. Mater. Chem. 16 (2006) 3558.
[82] G. Mehta, M.J. Kiel, J.W. Lee, N. Kotov, J.J. Linderman, S. Takayama, Adv. Funct. Mater. 17 (2007) 2701.
[83] T.C. Pappas, W.M.S. Wickramanyake, E. Jan, M. Motamedi, M. Brodwick, N.A. Kotov, Nano Lett. 7 (2007) 513.
[84] W.S. Jang, I. Rawson, J.C. Grunlan, Thin Solid Films 516 (2008) 4819.
[85] B.C. Ku, D. Froio, D. Steeves, D.W. Kim, H. Ahn, J.A. Ratto, A. Blumstein, J. Kumar, L.A. Samuelson, Presented at 4th Technical Symposium in Honor of Sukanti K. Tripathy, Lowell, MA, December 05, 2003.
[86] D.W. Kim, H.S. Choi, C. Lee, A. Blumstein, Y. Kang, Presented at 1st International Conference on Polymer Batteries and Fuel Cells (PBFC-1), Jeju Isl, South Korea, June 01–06, 2003.
[87] S.L. Westcott, N.A. Kotov, J.W. Ostrander, A.A. Mamedov, D.K. Reust, J.P. Roark, Presented at Nanotechnology Conference and Trade Show (Nanotech 2004), Boston, MA, March 07–11, 2004.
[88] J.L. Lutkenhaus, E.A. Olivetti, E.A. Verploegen, B.M. Cord, D.R. Sadoway, P.T. Hammond, Langmuir 23 (2007) 8515.
[89] A. Laschewsky, E. Wischerhoff, M. Kauranen, A. Persoons, Macromolecules 30 (1997) 8304.
[90] B. van Duffel, T. Verbiest, S. Van Elshocht, A. Persoons, F.C. De Schryver, R.A. Schoonheydt, Langmuir 17 (2001) 1243.

[91] D.W. Kim, A. Blumstein, S.K. Tripathy, Chem. Mater. 13 (2001) 1916.
[92] D.W. Kim, A. Blumstein, J. Kumar, S.K. Tripathy, Chem. Mater. 13 (2001) 243.
[93] I. Place, T.L. Penner, D.W. McBranch, D.G. Whitten, J. Phys. Chem. A 107 (2003) 3169.
[94] Z.H. Guo, Y. Shen, F. Zhao, M.K. Wang, S.J. Dong, Analyst 129 (2004) 657.
[95] X.W. Fan, J. Locklin, J.H. Youk, W. Blanton, C.J. Xia, R. Advincula, Chem. Mater. 14 (2002) 2184.
[96] F. Caruso, R.A. Caruso, H. Mohwald, Science 282 (1998) 1111.
[97] R.A. Caruso, A. Susha, F. Caruso, Chem. Mater. 13 (2001) 400.
[98] Z.H. Lu, S. Eadula, Z.G. Zheng, K. Xu, G. Grozdits, Y. Lvov, Colloid Surf. A-Physicochem. Eng. Asp. 292 (2007) 56.
[99] M.F. Yu, O. Lourie, M.J. Dyer, K. Moloni, T.F. Kelly, R.S. Ruoff, Science 287 (2000) 637.
[100] P. Calvert, Nature 399 (1999) 210.
[101] M.S. Dresselhaus, G. Dresselhaus, A. Jorio, Ann. Rev. Mater. Res. 34 (2004) 247.
[102] A. Jorio, R. Saito, J.H. Hafner, C.M. Lieber, M. Hunter, T. McClure, G. Dresselhaus, M.S. Dresselhaus, Phys. Rev. Lett. 86 (2001) 1118.
[103] A.M. Rao, E. Richter, S. Bandow, B. Chase, P.C. Eklund, K.A. Williams, S. Fang, K.R. Subbaswamy, M. Menon, A. Thess, R.E. Smalley, G. Dresselhaus, M.S. Dresselhaus, Science 275 (1997) 187.
[104] C. Fantini, A. Jorio, M. Souza, M.S. Strano, M.S. Dresselhaus, M.A. Pimenta, Phys. Rev. Lett. 93 (2004) 4.
[105] M.S. Dresselhaus, P.C. Eklund, Adv. Phys. 49 (2000) 705.
[106] B.S. Shim, Z.Y. Tang, M.P. Morabito, A. Agarwal, H.P. Hong, N.A. Kotov, Chem. Mater. 19 (2007) 5467.
[107] J.H. Rouse, P.T. Lillehei, Nano Lett. 3 (2003) 59.
[108] M. Olek, J. Ostrander, S. Jurga, H. Mohwald, N. Kotov, K. Kempa, M. Giersig, Nano Lett. 4 (2004) 1889.
[109] N.I. Kovtyukhova, T.E. Mallouk, J. Phys. Chem. B 109 (2005) 2540.
[110] N.L. Kovtyukhova, T.E. Mallouk, Adv. Mater. 17 (2005) 187.
[111] J.H. Rouse, P.T. Lillehei, J. Sanderson, E.J. Siochi, Chem. Mater. 16 (2004) 3904.
[112] W. Xue, T.H. Cui, Nanotechnology 18 (2007) 7.
[113] J.H. Shi, Y.J. Qin, H.X. Luo, Z.X. Guo, H.S. Woo, D.K. Park, Nanotechnology 18 (2007) 5.
[114] H. Paloniemi, M. Lukkarinen, T. Aaritalo, S. Areva, J. Leiro, M. Heinonen, K. Haapakka, J. Lukkari, Langmuir 22 (2006) 74.
[115] J.F. Shen, Y.Z. Hu, C. Qin, M.X. Ye, Langmuir 24 (2008) 3993.
[116] S.E. Moya, A. Ilie, J.S. Bendall, J.L. Hernandez-Lopez, J. Ruiz-Garcia, W.T.S. Huck, Macromol. Chem. Phys. 208 (2007) 603.
[117] B.S. Shim, J. Starkovich, N. Kotov, Compos. Sci. Technol. 66 (2006) 1174.
[118] T.R. Hendricks, J. Lu, L.T. Drzal, I. Lee, Adv. Mater. 20 (2008) 2008.
[119] G. Angelini, S. Boncompagni, P. De Maria, M. De Nardi, A. Fontana, C. Gasbarri, E. Menna, Carbon 45 (2007) 2479.
[120] E. Jan, N.A. Kotov, Nano Lett. 7 (2007) 1123.
[121] M.K. Gheith, T.C. Pappas, A.V. Liopo, V.A. Sinani, B.S. Shim, M. Motamedi, J.R. Wicksted, N.A. Kotov, Adv. Mater. 18 (2006) 2975.
[122] H.T. Ham, Y.S. Choi, M.G. Chee, M.H. Cha, I.J. Chung, Polym. Eng. Sci. 48 (2008) 1.
[123] K.J. Loh, J. Kim, J.P. Lynch, N.W.S. Kam, N.A. Kotov, Smart Mater. Struct. 16 (2007) 429.
[124] M.D. Shirsat, C.O. Too, G.G. Wallace, Electroanalysis 20 (2008) 150.
[125] S. Korkut, B. Keskinler, E. Erhan, Talanta 76 (2008) 1147.
[126] X. Wang, H.X. Huang, A.R. Liu, B. Liu, T. Wakayama, C. Nakamura, J. Miyake, D.J. Qian, Carbon 44 (2006) 2115.
[127] X. Wang, H.X. Huang, A.R. Liu, B. Liu, M. Chen, D.J. Qian, Thin Solid Films 516 (2008) 3244.
[128] L. Wang, S.J. Guo, X.O. Hu, S.J. Dong, Colloid Surf. A-Physicochem. Eng. Asp. 317 (2008) 394.
[129] Y.J. Zou, C.L. Xian, L.X. Sun, F. Xu, Electrochim. Acta 53 (2008) 4089.
[130] L.B. Koh, I. Rodriguez, J.J. Zhou, J. Biomed. Mater. Res. A 86A (2008) 394.
[131] D. Nepal, S. Balasubramanian, A.L. Simonian, V.A. Davis, Nano Lett. 8 (2008) 1896.
[132] N.Q. Jia, Q. Lian, H.B. Shen, C. Wang, X.Y. Li, Z.N. Yang, Nano Lett. 7 (2007) 2976.
[133] M. Palumbo, K.U. Lee, B.T. Ahn, A. Suri, K.S. Coleman, D. Zeze, D. Wood, C. Pearson, M.C. Petty, J. Phys. D-Appl. Phys. 39 (2006) 3077.
[134] W. Xue, Y. Liu, T.H. Cui, Appl. Phys. Lett. 89 (2006) 3.
[135] J.H. Yuan, Z.J. Wang, Y.J. Zhang, Y.F. Shen, D.X. Han, Q. Zhang, X.Y. Xu, L. Niu, Thin Solid Films 516 (2008) 6531.
[136] X. Yu, R. Rajamani, K.A. Stelson, T. Cui, Surf. Coat. Technol. 202 (2008) 2002.
[137] X. Yu, R. Rajamani, K.A. Stelson, T. Cui, Sens. Actuat. A-Phys. 132 (2006) 626.
[138] V. Jain, H.M. Yochum, R. Montazami, J.R. Heflin, L.B. Hu, G. Gruner, J. Appl. Phys. 103 (2008) 5.
[139] K.J. Loh, J.P. Lynch, B.S. Shim, N.A. Kotov, J. Intell. Mater. Syst. Struct. 19 (2008) 747.
[140] H.Y. Ma, L.P. Zhang, Y. Pan, K.Y. Zhang, Y.Z. Zhang, Electroanalysis 20 (2008) 1220.
[141] X.B. Yan, X.J. Chen, B.K. Tay, K.A. Khor, Electrochem. Commun. 9 (2007) 1269.
[142] B.Y. Wu, S.H. Hou, F. Yin, Z.X. Zhao, Y.Y. Wang, X.S. Wang, Q. Chen, Biosens. Bioelectron. 22 (2007) 2854.
[143] Y.Y. Sun, H.Y. Wang, C.Q. Sun, Biosens. Bioelectron. 24 (2008) 22.
[144] Y. Liu, S. Wu, H.X. Ju, L. Xu, Electroanalysis 19 (2007) 986.
[145] F.L. Qu, M.H. Yang, J.W. Chen, G.L. Shen, R.Q. Yu, Anal. Lett. 39 (2006) 1785.
[146] J. Zhang, M. Feng, H. Tachikawa, Biosens. Bioelectron. 22 (2007) 3036.
[147] Y.Z. Zhang, Y. Pan, S. Sit, L.P. Zhang, S.P. Li, M.W. Shao, Electroanalysis 19 (2007) 1695.
[148] M.N. Zhang, K.P. Gong, H.W. Zhang, L.Q. Mao, Biosens. Bioelectron. 20 (2005) 1270.
[149] Y.X. Liu, W.Z. Wei, Electrochem. Commun. 10 (2008) 872.
[150] H.H. Yu, T. Cao, L.D. Zhou, E.D. Gu, D.S. Yu, D.S. Jiang, Sens. Actuat. B-Chem. 119 (2006) 512.
[151] W. Xue, T.H. Cui, Presented at Workshop on Solid-State Sensors, Actuators and Microsystems, Hilton Head Isl, SC, June 04–08, 2006.
[152] T.J. Kang, M. Cha, E.Y. Jang, J. Shin, H.U. Im, Y. Kim, J. Lee, Y.H. Kim, Adv. Mater. 20 (2008) 3131.
[153] C.Y. Jiang, S. Markutsya, Y. Pikus, V.V. Tsukruk, Nat. Mater. 3 (2004) 721.
[154] M. Michel, A. Taylor, R. Sekol, P. Podsiadlo, P. Ho, N. Kotov, L. Thompson, Adv. Mater. 19 (2007) 3859.
[155] J. Shi, Y.Q. Hu, Y.X. Hua, Electroanalysis 20 (2008) 1483.
[156] L. Wang, S.J. Guo, L.J. Huang, S.J. Dong, Electrochem. Commun. 9 (2007) 827.
[157] W.F. Chen, J.S. Wu, P.L. Kuo, Chem. Mater. 20 (2008) 5756.
[158] L. Deng, L. Shang, Y.Z. Wang, T. Wang, H.J. Chen, S.J. Dong, Electrochem. Commun. 10 (2008) 1012.
[159] M. Sano, A. Kamino, J. Okamura, S. Shinkai, Nano Lett. 2 (2002) 531.
[160] L.J. Ji, J. Ma, C.G. Zhao, W. Wei, X.C. Wang, M.S. Yang, Y.F. Lu, Z.Z. Yang, Chem Commun. 11 (2006) 1206.
[161] J.H. Shi, Z.Y. Chen, Y.J. Qin, Z.X. Guo, J. Phys. Chem. C 112 (2008) 11617.
[162] B.S. Kim, B. Kim, K.D. Suh, J. Polym. Sci. Polym. Chem. 46 (2008) 1058.
[163] C. Pan, L.Q. Ge, Z.Z. Gu, Compos. Sci. Technol. 67 (2007) 3271.
[164] A.B. Artyukhin, O. Bakajin, P. Stroeve, A. Noy, Langmuir 20 (2004) 1442.
[165] N. Du, H. Zhang, B.D. Chen, X.Y. Ma, Z.H. Liu, J.B. Wu, D.R. Yang, Adv. Mater. 19 (2007) 1641.
[166] K.S. Liu, H.G. Fu, Y. Xie, L.L. Zhang, K. Pan, W. Zhou, J. Phys. Chem. C 112 (2008) 951.
[167] M.K. Gheith, V.A. Sinani, J.P. Wicksted, R.L. Matts, N.A. Kotov, Adv. Mater. 17 (2005) 2663.
[168] P.V. Pavoor, A. Bellare, A. Strom, D.H. Yang, R.E. Cohen, Macromolecules 37 (2004) 4865.